Stable structural and magnetic isomers of small transition-metal clusters from the Ni group: an *ab initio* density-functional study

2006 J. Phys.: Condens. Matter 18 9703

(http://iopscience.iop.org/0953-8984/18/42/016)

INSTITUTE OF PHYSICS PUBLISHING JOURNAL OF PHYSICS: CONDENSED MATTER

J. Phys.: Condens. Matter **18** (2006) 9703–9748 doi:10.1088/0953-8984/18/42/016

Stable structural and magnetic isomers of small transition-metal clusters from the Ni group: an *ab initio* density-functional study

T Futschek, J Hafner and M Marsman

Institut für Materialphysik and Center for Computational Materials Science, Universität Wien, Sensengasse 8/12, A-1090 Wien, Austria

Received 17 July 2006, in final form 12 September 2006
Published 6 October 2006
Online at stacks.iop.org/JPhysCM/18/9703

Abstract

We present *ab initio* density-functional studies of structural and magnetic isomers of Ni_N and Pt_N clusters with up to 13 atoms. Our investigations are based on fixed-moment calculations within a spin-polarized generalized gradient approximation and on static as well as dynamical optimizations of the cluster-structure, using quantum-mechanical many-body forces calculated via the Hellmann–Feynman theorem. Together with our earlier paper on Pd_N clusters (Futschek *et al* 2005 *J. Phys.: Condens. Matter* **17** 5927–63) the present work completes a comprehensive investigation of small clusters formed by metals of the Pt group of the periodic table. We discuss the trends in structure, binding energy and magnetic moments as a function of cluster size and through the 3d–4d–5d series. We demonstrate that the transition from the more localized 3d to the more extended 5d orbitals influences not only the magnetic ground state, but also the geometric structure of the clusters. The difference is most pronounced for the largest clusters in this series ($N = 11, 12, 13$) where the Ni clusters adopt a polytetrahedral arrangement converging to the Ni_{13} icosahedron, whereas the structures of Pd clusters and Pt clusters are based on octahedral motifs closely resembling fragments of the face-centred cubic structure of the bulk metals.

(Some figures in this article are in colour only in the electronic version)

M Supplementary data files are available from stacks.iop.org/JPhysCM/18/9703

1. Introduction

The last decade has witnessed the rapid development of a new field of research—nanoscience. This field stretches across physics, chemistry and engineering and addresses a vast number of important problems, ranging from fundamental science to promising technological applications. The purpose of nanoscience and nanotechnology is to produce, manipulate, control and understand objects measuring a few nanometres in diameter. The properties

of these nanosized objects often differ qualitatively both from those of their constituent atoms or molecules and from those of macroscopic materials. Among nanodimensional objects, nanoclusters occupy a very important place. Nanoclusters are aggregates of atoms or molecules, containing between less than 10 and 10^6 constituent particles [1, 2]. Possible applications of nanoclusters range from catalysis [3, 4] to spintronics [5].

In contrast to molecules, clusters have no fixed size or composition. They may be homogeneous (i.e. consist only of one type of atom or molecule), charged or neutral and held together by different types of chemical bonds. Strong electrostatic interactions stabilize NaCl clusters, van der Waals interactions bind the atoms in rare-gas clusters, covalent bonds dominate in Si clusters, metallic bonding in alkali- or noble-metal clusters. However, even the character of chemical bonding may be different at macroscopic and nanometric dimensions—there is increasing evidence that bonding in transition-metal clusters is more covalent than in the bulk metals. At the basis of any understanding of cluster properties is the investigation of their geometric structure. Being finite objects, nanoclusters are not subject to the constraints of translational invariance. Therefore, clusters can adopt noncrystalline structures such as icosahedra or decahedra. A further consequence of their small size is that nanoclusters have a very high surface/volume ratio. Hence the surface energy plays a very important role in determining the cluster structure.

It has been proposed [6, 7] that the binding energy E_b of a cluster built by N atoms can be written in the form

$$E_b = aN + bN^{2/3} + cN^{1/3} + d \tag{1}$$

where the first terms represents the volume contribution while the following terms correspond to surface contributions from facets, edges, and vertices. The optimal cluster structure results from the simultaneous optimization of volume and surface contributions to the binding energy. Evidently, for large clusters the volume contribution is optimized if the cluster structure is identical to that of the crystalline bulk material—in this case the parameter a is identical to the cohesive energy per atom. The surface contributions at fixed volume are optimized if the facets formed at the surface of the cluster obey the Wulff condition, i.e. for a face-centred cubic (fcc) structure

$$\frac{\gamma(100)}{\gamma(111)} = \frac{d100)}{d(111)} \tag{2}$$

where $\gamma(100)$ and $\gamma(111)$ are the (100) and (111) surface energies and $d(100)$ and $d(111)$ the distances of the facets from the centre of the cluster. The Wulff construction is a reliable tool for determining the shape of large clusters [6, 8], but for smaller clusters the aspherical Wulff shapes lead to a rather unfavourable energetics. In this case, quasispherical shapes based on icosahedral [9, 10] or decahedral [11] motifs may give lower energies. Icosahedral clusters are bounded by (111)-like facets only, decahedra by (100)-like facets; both optimize the surface/volume ratio but introduce large strain because radial bonds are compressed compared to intrashell bonds. In summary, icosahedral structures are expected to be favoured at small clusters sizes, while crystalline motifs dominate at large clusters. Decahedra could exist at intermediate sizes. Qualitatively, this scenario has been confirmed for a variety of different cluster types, ranging from rare-gas [12] to Cu [13], although it is evident that the icosahedral $\rightarrow$ decahedral $\rightarrow$ fcc crossover sizes are strongly material-dependent [14].

For metallic clusters in particular, geometric and electronic effects are often in competition. For clusters of alkali and noble metals where chemical bonding is promoted by free-electron-like s-electrons, the spherical-jellium model [15] predicts a high stability for clusters with closed electronic shells. For small alkali-metal clusters, several high-level quantum chemical calculations [16, 17] have demonstrated that electronic-shell closing is a better criterion for

stability than geometric packing, while for small Ag clusters it has been demonstrated [18] that both geometric and electronic effects play an important role. For transition-metal clusters, the situation is even more complex because the hybridization between the more delocalized s- and the tightly bound d-electrons leads to a metallo-covalent bonding describable only by complex many-body interactions. For the noble metals Cu, Ag, and Au and for the Pt-group transition metals Ni, Pd, and Pt, Baletto *et al* [7, 8] and Mottet *et al* [19] used the semiempirical potential of Rosato *et al* [20] to explore the cross-over between icosahedral, decahedral and fcc structures. Similar studies of Doyle and Wales [21] are based on the Sutton–Chen [22] potentials. Interestingly, while for the 3d-metals Cu and Ni icosahedral arrangements are predicted to represent the minimum-energy structures for clusters with up to 1000 atoms, the cross-over is located at less than 100 atoms for the 4d elements Ag and Pd and the 5d-metals Au and Pt. Since these results are based on semiempirical potentials optimized for bulk metals, these predictions must be considered with some reserve and should be checked against a higher level of theory. *Ab initio* calculations performed up to the year 2000 have been reviewed by Alonso [23]; more recent work is summarized in the review by Baletto and Ferrando [7]. Quantum chemical calculations for Cu_N ($N \leqslant 10$) [24] and Ag_N ($N \leqslant 9$) [25, 26] comparing the total energies for various structures found planar arrangements to be stable up to $N = 5$, in agreement with density-functional theory (DFT) calculations for Cu_N [27–30], Ag_N [31–35], and Au_N [36–39]. Only a few *ab initio* results are available for larger clusters. For neutral gold clusters and cluster anions with $N = 4$–14, Häkkinen *et al* [39] reported, on the basis of *ab initio* DFT calculations, a pronounced tendency of both neutral and anionic clusters to adopt a planar geometry up to $N = 12$. Although the energetic ordering of different structural isomers is not always the same for the neutral clusters and for the corresponding anions, the preference for planar geometries remains the same. The studies of Gilb *et al* [36] and Furche *et al* [37] based on a combination of DFT calculations and ion mobility measurements lead to a slightly different conclusion: while for anionic clusters, the preference for planar structures is confirmed up to $N = 14$, for cationic clusters, planar geometries are found only up to $N = 7$. However, Häkkinen *et al* note that DFT calculations tend to overestimate the stability of planar structures and that it is difficult to reconcile the photoelectron spectra calculated for planar isomers with $N \geqslant 8$ with the experimental results. Nonetheless, the more pronounced trend to find planar cluster structures for Au than for Ag and Cu seems to be confirmed—it will be interesting to see whether a similar tendency exists also for transition metals. For slightly larger Au cluster anions ($N = 16$–18) Bulusu *et al* [40] very recently reported experimental and theoretical evidence for cage-like hollow cluster structures.

For Cu_{13} the DFT results of Fujima and Yamaguchi [29] indicate that the icosahedron is more stable than the cuboctahedron, while for Ag_{13} Oviedo and Palmer [32] found a low-symmetry structure as the most stable isomer, and the cuboctahedron to be lower in energy than the icosahedron. In contrast to these results, Jennison *et al* found that even for $N = 55$ the Mackay icosahedron is energetically more favourable than the cuboctahedron. No systematic trend is recognizable, because all studies are restricted to a few selected cluster sizes and compare only structures created by a static relaxation of a few high-symmetry starting configurations. The only exceptions are the studies of Massobrio *et al* [30] on Cu_N ($N \leqslant 10$) and of Liu *et al* [35] on Ag_N ($N = 4, 5, 6$) based on *ab initio* molecular dynamics [41–43], confirming the preference for planar structures for the smallest noble-metal clusters (up to $N = 5$ for Ag_N). The resulting cluster geometries are generally less symmetric than the model structures considered in other *ab initio* studies. Au_N clusters have also been studied using *ab initio* methods. Planar structures represent the ground state up to $N = 6$ according to Bravo-Perez *et al* [44, 45] and Wang *et al* [46], and up to $N = 10$ according to Bonacic-Koutecky *et al* [47], in accordance with experimental studies of Gilb *et al* [36] on mass-selected clusters

with up to $N = 7$. The increased preference for planar structures compared to Cu_N and Ag_N has been attributed to relativistic effects (the 6s-level moving closer to the 5d-state) leading to a stronger s–d hybridization. For larger clusters, Li *et al* [48] and Wang *et al* [49] found computational and experimental evidence that Au_{20} is a tetrahedron.

For clusters formed by late transition-metals, magnetism adds to the complexity of the problem. Extensive Stern–Gerlach deflection measurements have demonstrated that not only in small superparamagnetic clusters of the 3d-metals Fe, Co, and Ni the magnetic moment is strongly enhanced over the value in the ferromagnetic bulk [50–54], but also clusters formed by the nonmagnetic 4d element Rh show superparamagnetic behaviour for $N \leqslant 60$ [55–57], while the magnetic ground state of Pd_N clusters remains controversial. The earlier Stern–Gerlach experiments [55–57] suggested the absence of magnetism, while photoemission experiments [58] indicated a Ni-like spin distribution at least for $N \leqslant 6$, excluding magnetic polarization only for $N \geqslant 15$. Susceptibility measurements [59] found nonvanishing magnetic moments even in much larger Pd_N clusters.

Very recently, we have published a comprehensive *ab initio* investigation [60] of the geometric and magnetic structures of Pd_N and Rh_N clusters with $N \leqslant 13$ (hereafter this work will be referred to as I). Extending earlier density-functional studies (Pd_N [61, 62], Rh_N [63, 64]—for further references we refer to I) of these clusters based on static optimizations of selected cluster structures, a dynamical simulated annealing approach is used to search for a global energy minimum. In addition, the spin-polarized DFT calculations have been performed in a fixed-moment mode to examine the possible coexistence of magnetic isomers and eventual magnetostructural effects. For all clusters with $N \geqslant 9$, the dynamical simulated annealing strategy has allowed to identify novel structures with a lower energy than any of the structural variants discussed previously in the literature: for $N = 9$ a double trigonal antiprism (similar to the canonical Bernal polyhedron for nine atoms); for $N = 11$ a structure consisting of two edge-sharing octahedra, completed by one adatom in a bridging position between two vertices; for $N = 12$ a similar configuration, but with two adatoms completing a third half-octahedron; and for $N = 13$ a cluster of three octahedra. Only for $N = 10$ are the ground-state configurations of Pd and Rh clusters different: Pd_{10} forms a structure consisting of two edge-sharing octahedra, while Rh_{10} adopts a configuration consisting of a tetragonal antiprism with capped square faces. The $N = 13$ atom structure has low symmetry (point group C_{1h}), it may also be considered as consisting of two fragments of close-packed layers, arranged in a close-packing stacking and slightly distorted at the edges. The polyoctahedral structures of the 12- and 11-atom clusters may be interpreted in a similar fashion. Independently of our work (but using the same computational approach), Chang and Chou [65] have found a very similar (but not identical, point group C_{2v}) 'buckled biplanar' structure to form the ground state for the 13-atom clusters of all 4d elements from Tc to Ag, while the clusters formed by the early transition metals (Y_{13}, Zr_{13}, Nb_{13}, Mo_{13}) prefer an icosahedral structure. The biplanar structures identified in I and in the work of Chang and Chou have lower average coordination number and shorter average bond length than the metastable distorted icosahedral configurations, it has been shown that these structures lead to an increased s–d hybridization (as measured by the hybridization index introduced by Häkkinen *et al* [38]) compared to the icosahedral clusters.

The fixed-moment calculations also reveal rather unexpected magnetic effects. Quite generally, magnetic energy differences are much smaller than structural energy differences—in many cases they are small enough to allow at finite temperatures for the coexistence of several magnetic isomers in thermal equilibrium. For certain clusters, the increasing probability to form a high-spin isomer may even lead to an increase of the average magnetization with temperature. Our study also presents evidence for coexisting ferro- and antiferromagnetic

components in the magnetization densities and for magnetostructural effects: examples are the Pd_3 triangle, the Pd_4 tetrahedron and the Pd_5 trigonal bipyramid where the $S = 0$ isomer is not paramagnetic, but antiferromagnetic; the Rh_6 octahedron where only the paramagnetic and the stable $S = 3$ high-spin isomers show full O_h symmetry, while the other magnetic isomers are tetragonally distorted; and the metastable Pd_{13} icosahedron which has I_h symmetry only in the high-spin limit, while the low-spin isomers undergo an orthorhombic distortion (symmetry C_{2h}). For both the Pd_{13} and Rh_{13} clusters the stable biplanar structure has a lower equilibrium magnetic moment than the icosahedron, improving the agreement with the Stern–Gerlach experiments [56, 57]. In a few cases (Rh_{11}, Rh_9), we have also found evidence for structure changes induced by a varying magnetization.

In the present work these investigations have been extended to Ni_N and Pt_N clusters with N up to 13, with the aim of elucidating the trends with the elements of the Pt group. Ni clusters have been investigated extensively, both experimentally [51–54, 66–73] and theoretically (reviews are found in [7] and [23]; further references are given below). The Stern–Gerlach experiments [51, 53] have found giant magnetic moments for the smallest Ni_N clusters, reaching a maximum of nearly three times the value in ferromagnetic fcc Ni for $N = 5$. Photoelectron spectra (PES) [58, 66–68, 70] show sharp molecular-like threshold structures for $N \leqslant 13$, merging with a broad band for larger clusters. It was concluded that for $N \leqslant 7$ no s–d hybridization occurs and that the 3d-orbitals are completely localized. In this regime the electronic structure and chemical binding in Ni_N clusters is similar to that of the corresponding Cu_N clusters. s–d hybridization starts with $N \geqslant 7$, and from $N = 10$ onwards the electronic states at the Fermi level show predominant d-character. Attempts have been made to correlate the structure in the PES to the geometric and magnetic properties of the clusters. For example, the spectrum of Ni_3 has been interpreted in terms of coexisting triangular and linear isomers, and the difference between the PES of Ni_{12} and Ni_{13} has been attributed to the higher (supposedly icosahedral) symmetry of the 13-atom cluster. However, it must be emphasized that these interpretations are largely speculative. The correlation between the PES and the magnetic properties is more convincing. The ground-state electron configuration of the Ni atom is $3d^84s^2$, but the $3d^94s^1$ configuration is only 0.025 eV higher in energy [74]. In bulk Ni and in large Ni_N clusters the electron configuration is $3d^94s^1$, limiting the spin contribution to the magnetic moment to $1\mu_B$, and for delocalized electrons the orbital moment is quenched. For the smallest ($N \leqslant 8$) clusters where the PES show evidence for a energetic separation of 4s- and 3d-derived molecular orbitals and for a strong localization of the Ni 3d-orbitals, Morenzin *et al* [70] discuss two possible mechanisms for the formation of the large magnetic moments: (i) an atomic-like $3d^84s^2$ electron configuration of the individual Ni atoms in the cluster (corresponding to a maximum spin moment of $2\mu_B$), or (ii) a predominant $3d^94s^1$ configuration, but in addition to the spin moment a large orbital component similar to free atoms or 4f-magnets. Hence the decrease of the magnetic moment with increasing cluster size would also signal a transition from localized to itinerant magnetism. Morenzin *et al* tend to dismiss mechanism (i) on energetic grounds.

In a series of studies Riley *et al* [71–73] (see also the review by Knickelbein [4] have probed the geometrical structure of Ni clusters via the adsorption of diatomic (N_2, CO) molecules. Structural information is derived from plateaus in the uptake-spectra, based on the idea (derived from studies of molecular adsorption on Ni surfaces) that each Ni atom on the cluster surface can bind one or two N_2 molecules rather weakly in an end-on configuration, binding of two molecules being confined to under-coordinated Ni atoms. Interpretation of CO adsorption studies is much more difficult because CO binds not exclusively in an atop configuration and the interaction is strong enough to eventually change the structure of the cluster. On the basis of the chemical probe method, the following cluster structures have

been proposed for Ni_N [4, 71–73, 75]: $N = 3$—triangle; $N = 4$—tetrahedron or square; $N = 5$—trigonal bipyramid; $N = 6$—octahedron; $N = 7$—capped octahedron; $N = 8$—bidisphenoid; $N = 9$—bicapped pentagonal bipyramid or tricapped trigonal prism; $N = 10$—tricapped pentagonal bipyramid; $N = 11$—?; $N = 12$—incomplete icosahedron; $N = 13$—icosahedron. However, it must be emphasized that for the interpretation of the uptake spectra, only a small number of seemingly evident high-symmetry configurations have been considered.

The structural, electronic and magnetic properties of Ni_N clusters have been investigated at different levels of theory. Quantum-chemical calculations (both at the Hartree–Fock (HF) and configuration–interaction (CI) levels) [76–78] and first-principles DFT studies [79–92] have been performed for selected geometries of the smallest clusters (up to $N = 8$ and for $N = 13$). Neither for the geometric nor for the magnetic ground state has a consensus between these different approaches been reached. Structural optimizations for small and larger clusters using dynamical simulated annealing techniques or molecular dynamics simulations have been performed within a tight-binding framework [93–98] or using parameterized force fields [99, 100]. Quite generally, these classical simulations lead to more compact structures than the *ab initio* approaches, and most of them ignore a possible interference between structural and magnetic stability.

Although supported Pt clusters have been investigated extensively because of their importance in catalysis (see, e.g., Ramaker *et al* [101]), only restricted information on free Pt clusters is available in the literature. Based on scanning transmission electron microscopy, Yeon-wook *et al* [102] and Contrata *et al* [103] reported a tendency to form disordered ('amorphous') structures in Pt clusters of different sizes. This finding is supported by DFT calculations by Yang *et al* [104] who found planar structures for Pt_N cluster with $N = 2$–6, and for Pt_{13} a variety of low-symmetry structures which are all lower in energy than the icosahedron or the cuboctahedron. A series of DFT calculations for clusters with up to seven Pt atoms [105–110] leads to conflicting results on the equilibrium geometries. For the Pt_{13} cluster Watari and Onishi [111] found the cuboctahedron, and Apra and Fortunelli [112] a decahedron as the ground-state configuration. Hence for this particular cluster, three DFT calculations [104, 111, 112] propose three different solutions. Very recently, Xiao and Wang [113] presented an extended comparative DFT study of the stability of linear, planar and three-dimensional structures for Pt_N clusters with $N = 2$–13 and $N = 19, 55$. Planar configurations are predicted to be stable for $N = 5$ and 6, while three-dimensional cluster geometries are predicted for $N = 4$ and $N \geqslant 7$. For the Pt_{13} cluster, a low-symmetry structure (point group C_s) was found to be lower in energy than a distorted icosahedron or cuboctahedron. Quantum-chemical *ab initio* calculations by Dai and Balasubramanian [114–116] predict three-dimensional structures for both the tetramer and the pentamer. More extended investigations of the structures of Pt clusters have been performed using classical molecular dynamics and thermal quenching simulations, based on force fields derived via an embedded-atom model [117–119].

The present work is devoted to *ab initio* DFT studies of structural and magnetic isomers of Ni and Pt clusters with up to 13 atoms, combining fixed moment calculations of the spin-polarized electronic structure and ground-state energy with static and dynamical structural optimizations based on exact quantum-mechanical many-body forces. Together with our previous results on Pd clusters, this completes a comprehensive investigation of clusters of all three metals of the Pt group of the Periodic Table and establishes characteristic common trends and differences between 3d, 4d, and 5d metals. Our paper is organized as follows. In section 2 we briefly review the theoretical foundations; sections 3 and 4 present our results for the geometric and magnetic structures of Ni_N and Pt_N clusters with $N \leqslant 13$. Section 5 summarizes the common trends for the three metals of the Pt group.

2. Computational method

All calculations were performed using the Vienna *ab initio* Simulation Package (VASP) [42, 43, 120, 121]. VASP is based on density-functional theory (DFT) theory and works in a plane wave basis set. The electronic ground state is determined by solving the Kohn–Sham equations using an iterative unconstrained band-by-band matrix diagonalization scheme based on a residual minimization method [120, 122]. Exchange and correlation were treated in the generalized gradient approximation (GGA), based on the parameterization by Perdew and Zunger [123] of the local-density functional of Ceperley and Alder [124], with the gradient corrections following Perdew and Wang [125]. Spin polarization was taken into account according to Von Barth and Hedin's [126] local-spin-density theory, using the spin interpolation proposed by Vosko *et al* [127]. The electron–ion interaction was described by the full-potential all-electron projector augmented wave (PAW) method, introduced by Blöchl [128], as implemented in VASP by Kresse and Joubert [129]. Our calculations have been performed in a scalar-relativistic mode (no spin–orbit coupling), although for the heavy element Pt a fully relativistic treatment seems to be required. This decision has a twofold motivation. (i) A consistent level of theory allows us to follow the trends through the Ni–Pd–Pt series independent of relativistic effects. (ii) Spin–orbit coupling strongly mixes different spin states, with two important consequences. First, no fixed-moment calculations are possible; hence we could not explore coexisting magnetic isomers and this would also hamper the structural optimizations. Second, as spin and orbital moments are not necessarily collinear, a noncollinear treatment of the magnetization densities would be required. For this reason, the investigation of relativistic effects on Pt_N clusters will be left to work in progress.

The plane-wave basis set included plane waves up to a kinetic energy cutoff of 250 eV. For clusters consisting of 2–10 atoms a $10 \times 10 \times 10$ Å^3 cubic supercell was used (this was found to be large enough to ensure that the periodically repeated cluster images do not interact with each other). For clusters consisting of more than 10 atoms per supercell a $15 \times 15 \times 15$ Å^3 cubic supercell was used. Electronic eigenstates have been calculated at the centre of the Brillouin zone of the supercell only. To improve convergence, a modest Gaussian smearing has been used for the calculation of the electronic density of states.

Our calculations have been performed in a fixed-moment mode [130, 131]. The total magnetic moment of the cluster is constrained to a fixed value by fixing the occupation numbers of the spin-up and spin-down channels. A fixed magnetic moment facilitates the structural optimizations and the availability of information on a series of magnetic isomers yields important information on magnetostructural effects. Local magnetic moments are calculated by projecting the plane-wave components of all occupied eigenstates onto spherical waves within slightly overlapping atomic spheres and integrating the resulting spin-polarized local densities of states up to the Fermi level. The radius of the spheres has been chosen such as to reproduce the correct total moment. However, due to the overlap of the spheres and the rather delocalized spin densities of low-spin isomers, a slight discrepancy between the total cluster moment and the sum over local atomic moments subsists in a few cases.

The geometry of the clusters has been determined by a static relaxation, using a conjugate-gradient minimization and the exact Hellmann–Feynman forces. For the smallest clusters (up to five atoms) a static optimization of the geometries of a few structural isomers was found to be sufficient, allowing several spin isomers (up to $S = 5$ for the smallest Ni clusters, up to $S = 7$ for larger cluster, and up to $S = 5$ for Pt clusters) for each structure. For larger clusters we performed in addition a dynamical simulated annealing [132, 133] of the cluster structure. Each simulated annealing runs starts with a molecular dynamic simulation at a high temperature of 1500 K, i.e. far above the melting temperature of the cluster. The system was

then gradually cooled down to room temperature before the final structural refinement using a static conjugated-gradient approach. For any further technical details we refer to I.

3. Geometric and magnetic structures of Ni_N clusters

In this section we discuss the structural and magnetic properties of Ni_N cluster for $N = 2$–13. To provide the background necessary for our discussions, we begin by briefly recapitulating the results available from various *ab initio* calculations and summarized in table 1.

The electronic structure and total energy of small Ni clusters ($N = 2$–8, 13) has been studied using quantum-chemical approaches at various levels of sophistication [76–78, 89], concentrating on the determination of the magnetic moment for a few fixed cluster geometries. The early HF-CI calculations of Basch *et al* [76] predict a linear geometry and a spin-quintet state for the Ni trimer, for the tetramer linear and square geometries with quintet and septet state, respectively, were found to be energetically degenerate and 0.14 eV/atom lower in energy than the tetrahedron. In contrast, in higher-level studies [77, 78] the tetramer was found to adopt a distorted tetrahedral geometry and a magnetic moment of 2.5 μ_B/atom (spin septet). The octahedral structure of the Ni_6 cluster also undergoes a Jahn–Teller distortion, the magnetic moment is 1.8 [1.5] μ_B/atom at the multireference CI (MRCI) and unrestricted Hartree–Fock (UHF) levels, respectively. For the Ni_{13} cluster O_h symmetry was preferred over I_h symmetry at both levels of approximation. The UHF calculations predict a magnetic moment of $0.7\mu_B$/atom, but no converged spin state could be found at the MRCI level.

A series of DFT calculations for Ni clusters with up to 13 atoms has been presented by the group of Reuse, Khanna *et al* [79–82]. For the Ni_4 cluster, the square and the distorted tetrahedron with a magnetic moment of 1.5 μ_B/atom are energetically degenerate, the stable structural isomers for Ni_5 and Ni_6 are a slightly distorted trigonal bipyramid and a octahedron, with magnetic moments of 1.6 μ_B/atom and $1\mu_B$/atom, respectively. Ni_7 forms a capped octahedron, Ni_8 a bidisphenoid, both with a total moment of $8\mu_B$; the icosahedron only was considered for Ni_{13}, yielding a bulk-like magnetic moment of $0.61\mu_B$/atom. The agreement with the structures derived from the N_2-uptake experiments is evident, but for each cluster only a few selected geometries have been considered. Other DFT calculations [83, 84] for selected geometries of small Ni_N clusters ($N \leqslant 6$) led to different results: for Ni_4 Castro *et al* also identified a Jahn–Teller distorted tetrahedron as the ground state, but the distortion is much weaker and the magnetic moment is only 1 μ_B/atom. Furthermore, a large energy difference with respect to a square geometry is reported, and the Ni_4-square is unstable against the formation of a rhombus. For Ni_5 both Castro *et al* and Michelini *et al* [84, 85] found the energy minimum for a trigonal bipyramid, but their calculated magnetic moment is only half as large ($0.8\mu_B$/atom) as that predicted by Reuse *et al*. For the Ni_6 cluster, Michelini *et al* found two energetically degenerate isomers in the form of a distorted octahedron, with D_{2h} and C_{2h} geometries and magnetic moments of 1.33 μ_B/atom (i.e. in this case larger than the result of Reuse *et al*).

The necessity to perform a global search for a structural minimum was addressed by a number of different studies. Nayak *et al* and Reddy [86, 87] used classical molecular dynamics (MD) based on an empirical many-body potential to generate equilibrium structures for Ni_N clusters with $N \leqslant 23$, followed by DFT calculations of the electronic and magnetic properties using both the local-density (LDA) and generalized gradient (GGA) approximations. For the smallest clusters with $N = 2$–6, the MD-optimized structures differ from the *ab initio* results by the absence of Jahn–Teller distortion, e.g., ideal tetrahedral and octahedral geometries are found for Ni_4 and Ni_6, respectively. The structures for Ni_7 and Ni_8 are formed by adding one or two atoms in front of a triangular facet of the Ni_6 octahedron (capped and bicapped octahedra). The

Table 1. Stable structure, point-group symmetry, average bond length ($\langle d \rangle$, in Å), and total spin S for small Ni_N clusters resulting from force-field (embedded atom–EAM) and *ab initio* (AI) calculations using DFT (LSDA, GGA) and quantum-chemical approaches (UHF, MRCI). Cf text.

N	Structure	Point group[a]	$\langle d \rangle$	S	Method	Reference
2	Dimer	$D_{\infty h}$	2.12	—	EAM	[99]
		$D_{\infty h}$	1.99	1	AI(LSDA)	[79]
		$D_{\infty h}$	2.13		AI(GGA)	[85]
		$D_{\infty h}$	2.17		AI(GGA)	[88]
		$D_{\infty h}$	2.10	1	AI(GGA)	[83]
		$D_{\infty h}$	2.33	1	AI(HF-CI)	[76]
3	Triangle	D_{3h}	2.25	—	EAM	[99]
		D_{3h}	2.26		AI(GGA)	[85]
		C_{2v}	2.15	1	AI(LSDA)	[79]
		D_{3h}	2.23	1	AI(GGA)	[83]
	Linear	$D_{\infty h}$	–	2	AI(HF-CI)	[76]
4	Tetrahedron	T_d	2.32	—	EAM	[99]
		$D_{2d}(\sim T_d)$	2.33		AI(GGA)	[85]
		D_{2d}/D_{4h}	2.17/2.10	3	AI(LSDA)	[79]
		S_4	2.21/2.41	2	AI(GGA)	[83]
	Linear/square	$D_{\infty h}/D_{4h}$	—	2/3	AI(HF-CI)	[76]
	tetrahedron	C_{3v}	2.30[b]	3/4	AI(MRCI)	[78]
5	Trig. bipyramid	D_{3h}	2.35	—	EAM	[99]
		D_{3h}	2.23/2.28	4	AI(LSDA)	[79]
		D_{3h}	2.31/2.36	2	AI(GGA)	[83]
		D_{3h}	2.31/2.39	2	AI(GGA)	[84]
	Square pyramid	C_{4v}	2.35		AI(GGA)	[85]
		C_{4v}	—	4	AI(HF-CI)	[76]
		C_{4v}	2.30	3	AI(MRCI)	[77]
6	Octahedron	O_h	2.36	—	EAM	[99]
		$C_i(\sim O_h)$	2.40		AI(GGA)	[85]
		C_{2h}	2.28/2.34	4	AI(GGA)	[84]
		D_{4h}	2.32/2.35	3	AI(LSDA)	[79]
		D_{4h}	2.36[b]	5	AI(MRCI)	[78]
7	Pentag. bipyramid	D_{5h}	2.39	—	EAM	[99]
		D_{5h}	2.28	3	AI(LSDA)	[86, 87]
	Capped octahedron	C_{3v}	2.27	4	AI (LSDA)	[81]
8	Bicap. octahedron	D_{2d}	2.38	—	EAM	[99]
	Bidisphenoid	$D_2(\sim D_{2d})$	2.26/2.30	4	AI(LSDA)	[81]
		D_{2d}	2.37		AI(GGA)	[90]
	Cube	O_h	2.16	4	AI(LSDA)	[79]
		O_h	2.25[b]	1	AI(MRCI)	[78]
		O_h	2.25[b]	5	AI(UHF)	[78]
13	Icosahedron	I_h	2.36/2.48	–	EAM	[99]
		I_h	2.23/2.34	4	AI(LSDA)	[79]
		I_h	2.39	4	AI(LSDA)	[86, 87]
		I_h	2.41/2.53		AI(GGA)	[88]
		I_h	2.49[b]	5	AI(UHF)	[78]
	Cube	O_h	2.41[b]	0	AI(MRCI)	[77]

[a] If the point-group symmetry quoted in this column is lower than the full symmetry of the structure given in the preceding column, the high-symmetry solution is unstable against distortions.
[b] No full structural optimization has been performed at the MRCI and UHF levels.

Ni_9 to Ni_{13} clusters evolve towards the icosahedral structure: Ni_9 forms a bicapped pentagonal bipyramid, the structures of Ni_{10} to Ni_{12} are formed by successively capping further triangular faces such that Ni_{12} is an icosahedron with an empty peripheral vertex. Except for Ni_{10} these results are in agreement with the structures derived from the N_2-adsorption experiments [4]. *Ab initio* calculations based on these structures yield good agreement with the experimental vertical ionization potentials, but magnetic moments substantially smaller than found in the experiments of Apsel *et al* [51] and Knickelbein [53], independently of the functional used in the calculations. Duan *et al* [91], also using structures generated by a parameterized dynamical simulated annealing approach [100] and subsequent DFT refinement, reported a cluster moment of $8\mu_B$ for $N = 5$–13, independent of the number of atoms and increasing to $16\mu_B$ for $N = 16$–24. Taken per atom, these magnetic moments are again much smaller than the experimental estimates. Ruette and Gonzalez [92] used a Monte Carlo simulated annealing algorithm, based on both a parameterized quantum chemical approach and a DFT calculation (using a hybrid functional), for a global structural optimization of the Ni_6 cluster. Both methods yield a lower energy for a pentagonal pyramid and for a capped trigonal bipyramid than for the octahedron.

Tight-binding molecular dynamics (TB-MD) studies of the structural, electronic and magnetic properties of Ni clusters have been performed by a number of groups [93–98]; for an extensive review of TB-based studies see also Alonso [23]. For the smallest clusters, the work of Andriotis *et al* [93] leads to geometric and magnetic structures in essential agreement with earlier DFT results [79, 80]; for the Ni_{13} cluster strong distortions from an icosahedral structure are predicted [93, 94]. Aguilera-Granja *et al* [95, 96] have emphasized the strong correlation between geometrical distortions and magnetic moment. Luo [97, 98] presented a series of TB-MD studies for clusters with up to 55 atoms (under the complete neglect of any magnetic effects), resulting in low-symmetry configurations for all $N \leqslant 11$, except for Ni_7 where a pentagonal bipyramid is found to be stable. Very recently, Grigoryan and Springborg [99] presented an extended investigation of the structure of Ni_N clusters for $2 \leqslant N \leqslant 150$, based on embedded atom potentials and their Monte Carlo based 'Aufbau/Abbau' method for a global sampling of configuration space. We take the results of this study as representative for classical force-field simulations and present a detailed confrontation of the results of force-field and *ab initio* simulations in table 1. Quite generally, the classical simulations lead to more symmetric, more compact cluster structures. Differences with respect to the *ab initio* results begin already for $N = 3$, where some (but not all) *ab initio* studies find the equilateral triangle to be unstable with respect to a Jahn–Teller distortion. Similarly, the Ni_4 tetrahedron is distorted, but the *ab initio* studies differ on the degree of symmetry breaking. The same also applies to the Ni_6 octahedron. For $N = 5$, either a trigonal bipyramid or a tetragonal pyramid is predicted at the first-principles level. Different structures are also predicted for $N = 7$ and 8 (capped octahedron versus pentagonal bipyramid and bicapped octahedron versus cube, respectively). In these the energy differences between the lowest structural isomers are only a few hundreds of an eV/atom.

We now present our own results. Table 2 summarizes the main results (point-group symmetry, total magnetic moment, average coordination number and bond lengths, HOMO–LUMO gap, binding energy, magnetic and structural energy differences) for all 166 isomers for which a full structural optimization has been performed. Additional information (lengths of all nearest-neighbour bonds, local magnetic moments) and graphical representation of all clusters may be found in the supporting information available from stacks.iop.org/JPhysCM/18/9703 and on our website. The point group symmetry has been determined by analysing the bond lengths and local magnetic moments, considering the finite numerical accuracy of our calculations. Differences in bond lengths up to 0.01 Å and differences in the local magnetic moments of up to 0.02 μ_B have been neglected. It must also

Table 2. Point-group symmetry (PGS), total magnetic moment M (in μ_B, magnetic order O (NM—nonmagnetic, AF—antiferromagnetic, FI ferrimagnetic, otherwise ferromagnetic), average coordination number N_C, average nearest-neighbour distance d (in Å), HOMO–LUMO gap E_g (in eV), and binding energy (in eV/atom) for structural and magnetic isomers of Ni_N clusters with $N = 2$–13. The last two columns list the magnetic energy differences ΔE_{mag} for each structural isomer, and the structural energy difference ΔE_{struct} (both in meV/atom) calculated for the respective magnetic ground state. A asterisk added to the PGS symbol indicates that the magnetic symmetry is lower than that of the geometric structure.

N	Structure	PGS	M	O	N_C	d	E_g	Binding energy	ΔE_{mag}	ΔE_{struct}
2	Dimer	$D_{\infty h}$	0	NM	1	2.09	0.3109	0.908	246	
		$D_{\infty h}$	2		1	2.08	0.1714	1.154	—	
		$D_{\infty h}$	4		1	2.14	0.0000	0.464	690	
3	Triangle	C_{2v}	0	NM	2	2.20	0.2565	1.499	77	
		C_{2v}	2		2	2.20	0.1138	1.575	—	
		C_{2v}	4		2	2.23	0.0357	1.422	147	
4a	Square	D^*_{4h}	0	AF	2	2.17	0.2677	1.660	105	
		D_{4h}	2		2	2.18	0.1294	1.705	59	
		D_{4h}	4		2	2.18	0.0571	1.739	25	
		D_{4h}	6		2	2.17	0.1379	1.764	—	113
4b	Rhombus	D_{2h}	0	AF	2.5	2.24	0.3492	1.704	160	
		D_{2h}	2		2.5	2.24	0.1315	1.768	96	
		D_{2h}	4		2.5	2.24	0.2304	1.864	—	14
		C_2	6		2.5	2.29	0.2224	1.705	159	
4c	Tetrahedron	C_{2v}	0	AF	3	2.29	0.2538	1.832	45	
		C_{2v}	2		3	2.28	0.0940	1.851	27	
		S_4	4		3	2.28	0.5115	1.878	—	—
		S_4	6		3	2.31	0.0181	1.747	130	
5a	Square pyramid	C_{4v}	0	AF	3.2	2.28	0.4373	2.029	100	
		C_{4v}	2	FI	3.2	2.29	0.2874	2.051	77	
		C_{4v}	4		3.2	2.28	0.0000	2.051	78	
		C_{4v}	6		3.2	2.28	0.1544	2.129	—	14
		C_{4v}	8		3.2	2.28	0.0497	2.030	98	
5b	Trigonal bipyramid	C_{1h}	0	AF	3.6	2.31	0.2780	2.064	78	
		D^*_{3h}	2		3.6	2.30	0.3111	2.090	53	
		D_{3h}	4		3.6	2.30	0.1905	2.143	—	—
		D_{3h}	6		3.6	2.30	0.0000	2.084	59	
5c	Flat trigonal bipyramid	D^*_{3h}	0	AF	2.8	2.28	0.0000	1.800	143	
		C_{3v}	2		2.8	2.29	0.3974	1.906	37	
		D_{3h}	4		2.8	2.26	0.1905	1.900	42	
		D_{3h}	6		2.8	2.25	0.0000	1.942	—	200
6b	Octahedron	C_{2v}	0	AF	4	2.32	0.2113	2.235	115	
		D_{4h}	2	FI	4	2.32	0.0000	2.235	115	
		O^*_h	4		4	2.32	0.2179	2.257	93	
		D_{4h}	6		4	2.32	0.2168	2.303	47	
		D_{4h}	8		4	2.32	0.0418	2.350	—	—
		D_{4h}	10		4	2.35	2.3393	2.022	328	
6c	Incomplete pentagonal bipyramid (PBP)	C_{2v}	0	AF	4	2.34	0.2731	2.198	91	
		C_{1h}	2	FI	4	2.33	0.1723	2.209	80	
		C_{1h}	4	FI	4	2.33	0.0901	2.249	39	
		C_{1h}	6		4	2.33	0.1166	2.288	—	61
6d	Square pyramid plus adatom	C_{1h}	0	AF	3.7	2.31	0.2016	2.192	94	
		C_{1h}	2	FI	3.7	2.30	0.1166	2.202	85	
		C_{1h}	4		3.7	2.30	0.0694	2.246	40	
		C_{1h}	6		3.7	2.30	0.0581	2.286	—	63
		C_{1h}	8		3.7	2.30	0.1421	2.244	42	

Table 2. (Continued.)

N	Structure	PGS	M	O	N_C	d	E_g	Binding energy	ΔE_{mag}	ΔE_{struct}
7a	Centred hexagon	D_{2h}	0	AF	3.4	2.29	0.0410	2.138	98	
		D_{2h}	2	FI	3.4	2.29	0.0411	2.161	75	
		D_{2h}	4	FI	3.4	2.29	0.0633	2.196	40	
		D_{2h}	6		3.4	2.29	0.0161	2.236	—	244
		D_{2h}	8		3.4	2.31	0.0433	2.185	52	
7b	Pentagonal bipyramid (PBP)	C_{2v}	0	AF	4.6	2.36	0.2022	2.387	60	
		C_{2v}	2	FI	4.6	2.35	0.0635	2.357	90	
		C_{2v}	4		4.6	2.35	0.0412	2.381	67	
		C_{2v}	6		4.6	2.35	0.0773	2.447	—	33
		C_{2v}	8		4.6	2.36	0.1110	2.432	15	
7c	Octahedron with capped triangular face	C_{1h}	0	AF	4.3	2.36	0.1601	2.375	105	
		C_{3v}	2	FI	4.3	2.34	0.1645	2.418	62	
		C_{3v}	4	FI	4.3	2.35	0.0518	2.416	64	
		C_{1h}	6		4.3	2.33	0.060	2.433	47	
		C_{3v}	8		4.3	2.35	0.1198	2.480	—	—
		C_{3v}	10		4.3	2.35	0.1465	2.315	165	
8a	Bicapped octahedron I	C_{2v}	0	AF	4.5	2.34	0.1076	2.474	88	
		C_{2v}	2	FI	4.5	2.34	0.1684	2.474	88	
		C_{2v}	4	FI	4.5	2.34	0.0778	2.484	78	
		C_{2v}	6		4.5	2.34	0.1139	2.531	31	
		C_{2v}	8		4.5	2.33	0.0000	2.562	—	8
		C_{2v}	10		4.5	2.34	0.1864	2.450	111	
8b	Bicapped octahedron II (Bidisphenoid)	S_4	0	AF	4.5	2.35	0.1567	2.498	80	
		S_4	2	FI	5	2.40	0.2361	2.510	68	
		S_4	4		5	2.40	0.0547	2.507	71	
		C_{2v}	6		4.5	2.36	0.0845	2.542	35	
		C_{2v}	8		4.5	2.36	0.0619	2.578	—	—
		S_4	10		4.8	2.38	0.0542	2.465	113	
9a	Capped PBP	C_{1h}	0	AF	5.1	2.38	0.0935	2.555	88	
		C_{1h}	2	FI	5.1	2.37	0.0000	2.579	64	
		C_{1h}	4	FI	5.1	2.37	0.0178	2.592	56	
		C_{1h}	6	FI	5.1	2.37	0.0562	2.617	26	
		C_{1h}	8		5.1	2.36	0.0266	2.643	—	—
		C_{1h}	10		5.1	2.37	0.0000	2.572	70	
9b	Double trigonal antiprism (DTA)	D_{3h}	0	AF	4.7	2.34	0.1593	2.560	81	
		C_{2v}	2	FI	4.7	2.34	0.0000	2.575	65	
		D_{3h}	4	FI	4.7	2.34	0.2595	2.580	60	
		C_{2v}	6		4.7	2.34	0.0583	2.596	43	
		D_{3h}	8		4.7	2.33	0.0000	2.640	—	3
		D_{3h}	10		4.7	2.34	0.2347	2.590	51	
10a	Tetragonal antiprism with capped square faces	C_{4v}	0	AF	4.8	2.35	0.2139	2.658	31	
		C_{4v}	2	FI	4.8	2.35	0.1318	2.640	50	
		C_{4v}	4	FI	4.8	2.34	0.0617	2.631	58	
		C_{4v}	6		4.8	2.34	0.1318	2.646	43	
		C_{4v}	8		4.8	2.35	0.0422	2.680	—	73
		C_{4v}	10		4.8	2.35	0.0000	2.675	14	
10b	Edge-sharing double octahedra	D_{2h}	0	AF	5	2.35	0.0484	2.606	87	
		D_{2h}	2	FI	5	2.35	0.1387	2.605	88	
		D_{2h}	4	FI	5	2.35	0.0249	2.633	60	
		D_{2h}	6		5	2.35	0.0572	2.658	34	
		D_{2h}	8		5	2.35	0.0952	2.693	—	64
		D_{2h}	10		5	2.35	0.0235	2.671	21	

Table 2. (Continued.)

N	Structure	PGS	M	O	N_C	d	E_g	Binding energy	ΔE_{mag}	ΔE_{struct}
10c	Tetrahedron	C_{2v}	0	AF	4.8	2.35	0.1499	2.664	79	
		C_{1h}	2	FI	4.8	2.35	0.1327	2.676	80	
		C_{1h}	4	FI	4.8	2.35	0.2817	2.693	64	
		C_{1h}	6		4.8	2.34	0.2321	2.712	45	
		T	8		4.8	2.34	0.2820	2.757	—	—
		C_{1h}	10		4.8	2.34	0.0435	2.656	101	
11a	Polytetrahedral cluster	C_{2v}	0	AF	5.5	2.37	0.0340	2.727	74	
		C_{2v}	2	FI	5.5	2.37	0.0000	2.722	79	
		C_{2v}	4	FI	5.5	2.37	0.1276	2.736	65	
		C_{2v}	6		5.5	2.37	0.0522	2.755	46	
		C_{2v}	8		5.5	2.37	0.1154	2.801	—	—
		C_{2v}	10		5.5	2.37	0.0438	2.729	72	
11b	Edge-sharing octahedra plus adatom	C_1	0	AF	5.1	2.38	0.0230	2.721	39	
		C_1	2	FI	5.1	2.38	0.0766	2.709	50	
		C_1	4	FI	5.1	2.35	0.0831	2.718	43	
		C_1	6	FI	5.1	2.37	0.1190	2.731	29	
		C_1	8		5.1	2.37	0.0405	2.760	—	41
		C_1	10		5.1	2.36	0.0195	2.747	13	
12a	Capped cube	D_{4h}	2	FI	4.7	2.33	0.0871	2.685	54	
		D_{4h}	4		4.7	2.32	0.0595	2.680	59	
		D_{4h}	6		4.7	2.32	0.0831	2.700	39	
		D_{4h}	8		4.7	2.33	0.0000	2.725	14	
		C_{2h}	10		4.7	2.34	0.0483	2.739	—	81
		C_{2h}	12		4.7	2.34	0.0402	2.698	42	
12b	Incomplete icosahedron	C_{1h}	2	FI	6	2.40	0.0670	2.767	53	
		C_{1h}	4	FI	6	2.40	0.1118	2.771	48	
		C_{1h}	6		6	2.39	0.0451	2.787	33	
		C_{5v}	8		6	2.39	0.0901	2.820	—	—
		C_{1h}	10		6	2.40	0.0872	2.783	37	
12c	Edge-sharing octahedra plus two adatoms	C_1	2	FI	5.3	2.36	0.0872	2.727	63	
		C_1	4	FI	5.3	2.37	0.0436	2.758	31	
		C_{1h}	6	FI	5.3	2.36	0.0912	2.762	27	
		C_{1h}	8		5.3	2.36	0.0400	2.789	—	31
		C_{1h}	10		5.3	2.36	0.0532	2.785	4	
12d	Pyramid	C_{1h}	0	AF	5.3	2.37	0.0646	2.759	51	
		C_{1h}	2	FI	5.3	2.37	0.0311	2.762	48	
		C_{1h}	4	FI	5.3	2.37	0.0614	2.771	39	
		C_{1h}	6	FI	5.3	2.36	0.0499	2.781	29	
		C_{2v}	8		5.3	2.36	0.0606	2.810	—	10
		C_{2v}	10		5.3	2.37	0.0000	2.781	29	
13a	Capped cube with central atom	D_{2h}	0	AF	5.5	2.37	0.0560	2.760	44	
		D_{2h}	2	FI	5.5	2.37	0.0392	2.761	42	
		D_{2h}	4	FI	5.5	2.36	0.0424	2.761	43	
		D_{4h}	6	FI	5.5	2.36	0.0000	2.780	24	
		D_{2h}	8		5.8	2.42	0.1332	2.783	21	
		D_{2h}	10		5.8	2.42	0.0551	2.804	—	71
		D_{2h}	12		5.2	2.36	0.0813	2.795	9	
13b	Centred icosahedron	C_{1h}	0	AF	6.5	2.41	0.0869	2.819	56	
		C_{1h}	2	FI	6.5	2.40	0.1926	2.817	58	
		I_h	4	FI	6.5	2.40	0.1998	2.824	51	
		C_{1h}	6	FI	6.5	2.41	0.0000	2.851	24	
		C_{1h}	8		6.5	2.41	0.0000	2.875	—	—
		C_{1h}	10		6.5	2.41	0.0420	2.841	34	

Table 2. (Continued.)

N	Structure	PGS	M	O	N_C	d	E_g	Binding energy	ΔE_{mag}	ΔE_{struct}
13c	Cluster of octahedra	C_{1h}	2	FI	5.5	2.37	0.0465	2.788	56	
		C_{1h}	4	FI	5.5	2.37	0.0296	2.819	25	
		C_{1h}	6		5.5	2.36	0.1288	2.810	33	
		C_{1h}	8		5.5	2.37	0.0276	2.837	7	
		C_{1h}	10		5.5	2.37	0.0833	2.840	4	
		C_{1h}	12		5.5	2.37	0.0635	2.844	—	31
		C_{1h}	14		5.5	2.37	0.1109	2.815	28	
13d	Centred	D_{3h}	0	AF	5.5	2.37	0.1723	2.762	20	
	cuboctahedron	C_{2v}	2	FI	5.5	2.37	0.0000	2.764	17	
		C_{2v}	4	FI	5.5	2.36	0.0407	2.765	16	
		C_{2v}	6	FI	5.5	2.36	0.0000	2.781	—	94
		C_{2v}	8	FI	5.5	2.37	0.0000	2.772	9	
		C_{2v}	10		5.5	2.38	0.0615	2.751	30	

been emphasized that for low-spin isomers and low-symmetry configurations, the calculations of local magnetic moments based on projections of the eigenstates onto overlapping atomic spheres eventually leads to results that do not add up to the correct total magnetic moment derived from the spin-polarized densities of states. We begin by discussing the results for the individual clusters, followed by the analysis as a function of cluster size.

3.1. Ni_N clusters, $N = 2$–5—planar versus three-dimensional structures

3.1.1. Ni_2. For the Ni dimer we find the ground state to be a spin triplet ($S = 1$) with a bond length of 2.08 Å and a binding energy of 1.15 eV/atom. The nonmagnetic ($S = 0$) and the high-spin ($S = 2$) states are disfavoured by large magnetic energy differences of 0.25 eV/atom and 0.69 eV/atom, respectively. The bond length calculated for the singlet state is expanded by 0.01 Å, for the quintet state by 0.06 Å relative to the ground state. The experimental [134–136] bond length is 2.15 Å, the binding energy 1.03 eV/atom. Earlier quantum-chemical and DFT calculations for homonuclear transition-metal dimers have been compiled by Barden *et al* [89]. For Ni_2, the calculated bond lengths vary between 2.06 Å (LSDA), 2.11 to 2.16 Å using various gradient corrected functionals, 2.30 Å using a hybrid (B3LYP) functional, and 2.90 Å for unrestricted Hartree–Fock calculations. Reuse *et al* [79] predict $d = 1.99$ Å (LSDA); other GGA results are $d = 2.13$ Å [85] and $d = 2.17$ Å [88]. The calculated LSDA values for the binding energy are 1.61 eV/atom [79] and 1.74 eV/atom [89], the best GGA values reported by Barden *et al* range between 1.15 and 1.25 eV/atom. Hence it is evident that a gradient-corrected functional is necessary to correct for the overbinding of the LSDA. All DFT and quantum chemical calculations agree on a triplet ground state.

3.1.2. Ni_3. For the Ni trimer it is still a subject of debate whether the ground-state configuration is an equilateral or an isosceles triangle resulting from a Jahn–Teller distortion (cf table 1). We find the ground state to be a spin triplet ($S = 1$) with only a minimal distortion from threefold symmetry (the difference between the two long (2.21 Å) and the one short (2.20 Å) bond lengths is only 0.01 Å); the binding energy is 1.58 eV/atom. A stronger geometric distortion (bond-length difference 0.07 Å), coupled to a difference in the local magnetic moments (1.23, 1.23 and 1.53 μ_B) is found for the high-spin isomer ($S = 2$) which is 0.15 eV/atom higher in energy. The spin of $S = 1$ is in agreement with early measurements performed using a matrix isolation technique [137]. Reuse *et al* predict a slightly stronger

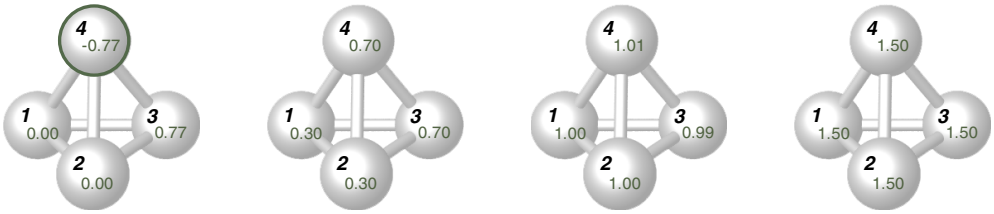

Figure 1. Structure and local magnetic moments of Ni_4 clusters with the structure of a distorted tetrahedron and $S = 0$–3. The interatomic distances are: $S = 0$—point-group symmetry (PGS) C_{2v}, $d_{12} = 2.22$ Å, all others $d_{ij} = 2.30$ Å; $S = 1$—PGS C_{2v}, $d_{12} = 2.36$ Å, all others $d_{ij} = 2.27$ Å; $S = 2$—PGS S_4, $d_{12} = d_{34} = 2.20$ Å, all other $d_{ij} = 2.32$ Å; $S = 3$—PGS S_4, $d_{12} = d_{34} = 2.49$ Å, all other $d_{ij} = 2.22$ Å. Atoms with negative magnetic moments are highlighted by a dark rim.

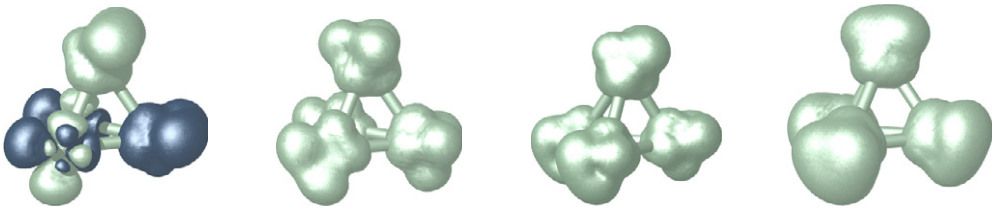

Figure 2. Isosurfaces of the magnetization densities of distorted tetrahedral Ni_4 clusters with $S = 0$–3. Light surfaces represent positive (spin-up), dark surfaces negative (spin-down) magnetization densities. Cf text.

geometric distortion ($\Delta d = 0.04$ Å), at a shorter bond length and higher binding energy due to their use of the LSDA. The GGA calculations of Michelini *et al* [85] predict a D_{3h} geometry and a larger bond length of 2.26 Å. Quantum-chemical calculations at the HF-CI level [76] predict a linear geometry and an $S = 2$ ground state.

3.1.3. Ni_4. For the Ni tetramer there is a competition between planar (square, rhombus) and three-dimensional (tetrahedron) geometries. We have used all three structures as starting configurations for our structural optimizations, with spins ranging between $S = 0$ and 3. We find the ground state to be a spin quintet ($S = 2$) with the structure of a distorted tetrahedron, but the second Ni_4 isomer (a rhombus with $S = 2$) is only 14 meV/atom higher in energy, while the structural energy difference of a regular Ni_4 square (adopting a $S = 3$ state) is 113 meV/atom. For the two nearly degenerate isomers, the structural distortion is coupled to the magnetic state. For the low-spin states ($S = 0, 1$) of the Ni_4 tetrahedron the symmetry is reduced to C_{2v} with two strongly and two weakly magnetic sites, and a distance between the low-moment sites which is about 0.08 Å shorter ($S = 0$) or longer ($S = 1$) than the remaining interatomic distances. In the high-spin ($S = 2, 3$) isomers all four sites are magnetically equivalent and the point-group symmetry is S_4, with two short bond lengths (2.20 Å) at opposite edges and four long bonds (2.32 Å) (see figure 1 for details). Similarly, for the rhombus the point-group symmetry is lowered from D_{2h} ($S = 0$–2) to C_2 for the magnetic ground state ($S = 3$).

It is also remarkable that the $S = 0$ state of both low-energy isomers is not nonmagnetic, but antiferromagnetic. Figure 2 shows isosurfaces of the magnetization densities for all four magnetic isomers of a distorted Ni_4 tetrahedron. In the singlet state, two Ni atoms carry moments of $\pm 0.77 \mu_B$, while the other two have zero moment. However, the analysis of the magnetization densities shows that even on the seemingly nonmagnetic sites the electron density has mutually orthogonal components with positive and negative spin polarization.

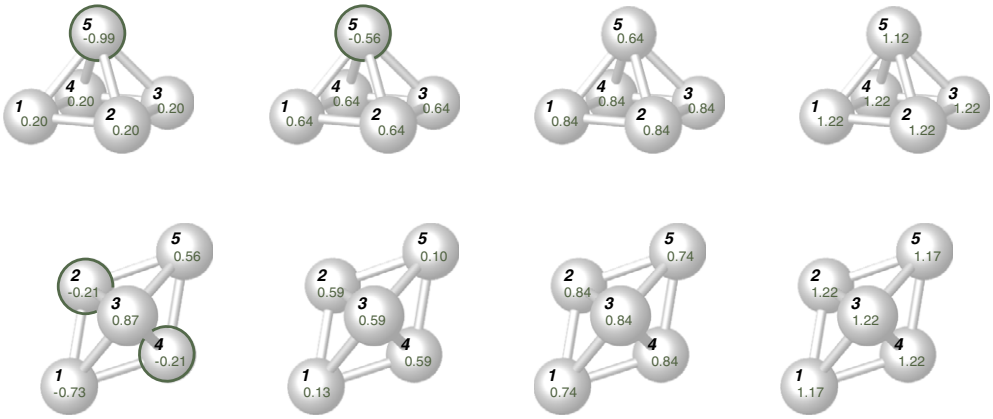

Figure 3. Structure and local magnetic moments of Ni_5 clusters with the structure of a square pyramid (top) and a trigonal bipyramid (bottom). The point-group symmetry is always C_{4v} for the square pyramid, while for the $S = 0$ isomer of the trigonal bipyramid the symmetry is reduced from D_{3d} to C_1. For the $S = 1$ isomer, the geometric structure has D_{3h} symmetry, but the magnetic symmetry is only C_{3v}. Cf text.

Our results for the Ni_4 cluster agree qualitatively with the GGA calculations of Michelini *et al* [85] who reported a slightly distorted nearly tetrahedral ground state, but differ appreciably from the LSDA results of Reuse *et al* [79] finding a distorted tetrahedron and a square to be energetically degenerate while we find a structural energy difference of 0.11 eV/atom. Also, Reuse *et al* predict a spin septet to be stable in both geometries. We confirm this result for the square, while $S = 2$ is the ground state for the distorted tetrahedron, in agreement with both the GGA and LSDA results of Castro *et al* [83]. The results of quantum-chemical calculations scatter rather widely. At the HF-CI level linear and planar (square) geometries are found to be preferred over the tetrahedron, with $S = 2, 3$ spin states. According to the calculations of Estiu *et al* [78] performed at the MRCI and UHF levels, septet and nonet states compete for the lowest energies, in agreement with the general tendency of Hartree–Fock-based approaches to produce a much larger exchange splitting than DFT calculations. Although these results do not refer to completely optimized geometries, they indicate that for the localized magnetism of the smallest Ni clusters (cf the discussion above) quantum-chemical and DFT approaches possibly lead to different results.

On the basis of the molecular adsorption experiments [4], the tetrahedral and planar structure are equally likely for the Ni tetramer—this agrees with our prediction of a small structural energy difference.

3.1.4. Ni_5. The evident structural isomers of the Ni_5 are a trigonal bipyramid and a square pyramid—both have been predicted to represent the ground state by *ab initio* calculations. Our results predict a small energy difference of 14 meV/atom between an acute trigonal bipyramid in an $S = 2$ state (which is also the stable structure according to the N_2 uptake experiments [4]) and a tetragonal pyramid in a $S = 3$ state. The magnetic energy differences are larger than this structural energy difference, and for the low-spin isomers we find a strong antiferromagnetic coupling between large local moments (see figure 3; for the square pyramid the $S = 1$ isomer has a ferrimagnetic structure. In addition, we have found a third metastable structural isomer in the form of a flat trigonal bipyramid.

Our prediction of a stable trigonal bipyramid agrees with Reuse *et al* [79], Michelini *et al* [84], Duan *et al* [91] and Castro *et al* [83], but there are considerable differences concerning

the stable magnetic isomer. While Reuse *et al* and Duan *et al* predict a total magnetic moment of $8\mu_B$ (spin nonet), we agree with Michelini *et al* and Castro *et al* in finding a moment of only $4\mu_B$ (spin quintet). A high-spin state (septet) has been found in the MRCI and UHF calculations of Estiu *et al* [78] for both C_{4v} and D_{3h} symmetries, but with the tetragonal pyramid (C_{4v}) favoured by a huge structural energy difference. For the C_{4v} geometry Basch *et al* [76] predict a spin nonet to represent the ground state. The experimental study of Apsel *et al* [51] reports a large moment of $8\mu_B$ (spin nonet). It remains unclear why the LSDA calculations of Reuse and Khanna [79] predict a magnetic moment which is twice as large as that resulting from all GGA calculations (in contrast to the general trend of the GGA to favour magnetization more strongly than the LSDA) and even larger than the UHF moment. Hence the large magnetic moment deduced from the Stern–Gerlach experiments [51] is reproduced by some of the older DFT and UHF calculations, while more recent *ab initio* studies report much smaller moments.

3.2. Ni_N clusters, $N = 6$–8—*octahedral structures*

While for the Ni_6 cluster there is a general consensus that an octahedral structure (as the smallest possible fragment of an fcc crystal) is preferred, it remains unclear whether the structure of 7- and 8-atom clusters is derived from the octahedron by adding atoms capping the triangular faces or whether structures built on noncrystallographic motifs are favoured. Already for this cluster size it is excluded to explore all possible configurations by static optimizations, dynamical simulations have proved to be particularly valuable.

3.2.1. Ni_6. We have explored four different configurations: pentagonal pyramid (6a), octahedron (6b), incomplete pentagonal bipyramid (one atom in the central plane is missing—6c), and square pyramid with a capped triangular face (6d). Configuration (6a) turns out to be unstable versus transformation into (6c)—one atom from the pentagonal basis moves out of the plane to form the second vertex of a pentagonal bipyramid (PBP). This structure is energetically almost degenerate with a capped square prism (6d)—both structures are appreciably distorted (point group C_{1h}) for most magnetic isomers and about 60 meV/atom higher in energy than a distorted octahedron. The geometric distortions of the Ni_6 octahedron are coupled to magnetostructural effects. The $S = 0$ isomer is antiferromagnetic with C_{2v} symmetry (see figure 4); the $S = 1$ state is ferrimagnetic with small negative moments on the sites forming the central plane and large positive moments on the remaining two vertices: the symmetry increases to D_{4h}. The geometric structure of the $S = 2$ isomer shows full octahedral symmetry (O_h), but the magnetic symmetry is only D_{4h} because the moments on the sites located on the fourfold axis carry moments which are more than twice as large than on the sites located in the central plane. The $S = 3$–5 configurations show D_{4h} symmetry; for the stable $S = 4$ isomer the local moments on all six sites are nearly equal (i.e. compatible with full O_h symmetry), but the tetragonal distortion leads to differences in the bond lengths of 0.04 Å.

Previous *ab initio* calculations all agree on a distorted octahedral geometry of the Ni_6 cluster, but the predictions for the magnetic moment scatter between $M = 6\mu_B$ (LSDA calculations of Reuse and Khanna [79]) and $M = 10\mu_B$ (HF-CI calculations of Basch *et al* [76] and MRCI calculations of Estiu *et al* [78]). The Stern–Gerlach experiments [51] yield a total moment of $M \sim 8\mu_B$ falling between the predictions of DFT and MRCI theories.

3.2.2. Ni_7. LSDA calculations for the Ni_7 cluster have found either a pentagonal bipyramid [86] or a capped octahedron [81] as the ground state. We have examined these

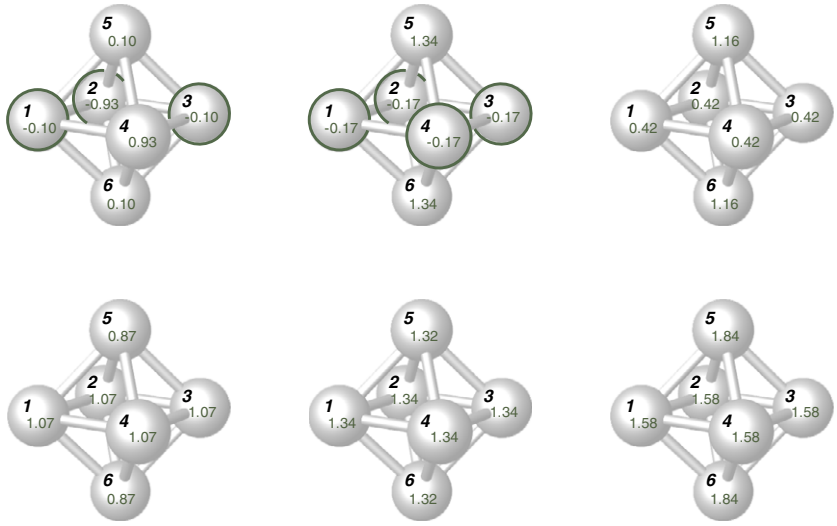

Figure 4. Structure and local magnetic moments of different magnetic isomers of Ni_6 clusters forming a distorted octahedron: $S = 0$—point-group symmetry C_{2v}, $S = 1$—D_{4h}, $S = 2$—O_h, $S = 3$–5—D_{4h}; cf text.

two geometries and in addition a planar arrangement, a centred hexagon. The ground state is the capped octahedron with $S = 4$, which is 33 meV/atom lower in energy than the pentagonal bipyramid with $S = 3$ and 244 meV/atom lower than the planar configuration with $S = 3$. All three configurations are appreciably distorted. For the bipyramid, the pentagonal symmetry is reduced to C_{2v}; for the centred hexagon the symmetry is D_{2h}, irrespective of the magnetic moment.

Interesting magnetostructural effects are observed for the stable structural isomer; see figure 5. For the low-spin isomers with $S = 0-2$ we find a strong antiferromagnetic component in the magnetic structure. The $S = 0$ state is antiferromagnetic; the symmetry is reduced to C_{1h} with a mirror plane through the capping atom. In contrast, for the ferrimagnetic $S = 1$ and 2 isomers, the symmetry is trigonal (C_{3v}); it can also be described as a trigonal antiprism with a capped basal plane. For spin state $S \geqslant 3$, the local magnetic moments are positive; for $S = 3$ the symmetry is again reduced to C_{1h}. For the $S = 4$ ground state, trigonal symmetry is recovered and the central Ni_6 unit shows nearly perfect octahedral symmetry in its geometry and local magnetic moments.

Our prediction of the structural and magnetic ground state $S = 4$ agrees with Desmarais *et al* [81] and Duan *et al* [91], but our GGA calculations produce a lower binding energy and higher bond length than the LSDA. The LSDA calculations of Reddy *et al* [87] predict $S = 3$ to represent the magnetic ground state; larger magnetic moments close to the experimental result [51] result only from the semi-empirical TB studies [93, 95, 96].

3.2.3. Ni_8. For the Ni_8 cluster the starting structures for the static optimizations consisted of bicapped octahedra, with the two capping atoms placed on opposite triangular faces, either with both capping atoms on one side of the central square of the octahedron (configuration 8a) or on opposite sides (configuration 8b) see figure 6. Configuration 8b is also describable as a bidisphenoid (or a pentagonal bipyramid with one atom in the basal plane replaced by a dimer). Dynamical simulated annealing also leads to configuration 8b, which is only

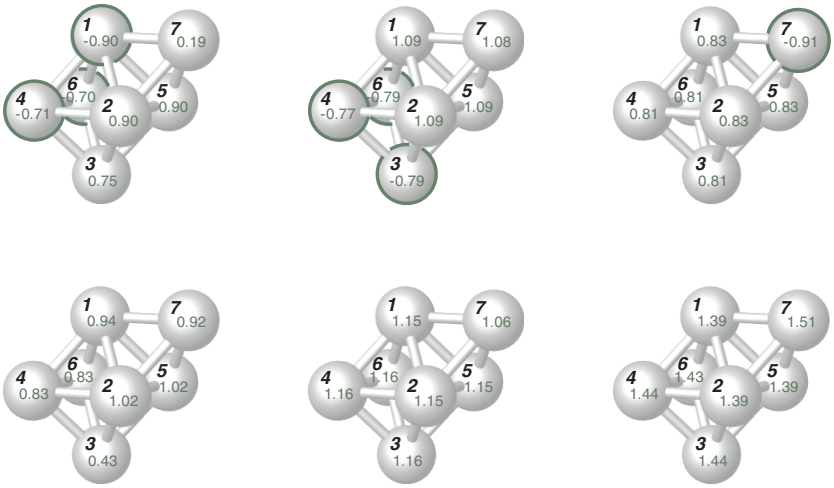

Figure 5. Structure and local magnetic moments of Ni_7 clusters forming a distorted capped octahedron: $S = 0$—C_{1h}, $S = 1, 2$—C_{3v}, $S = 3$—C_{1h}, $S = 4, 5$—C_{3v}; cf text.

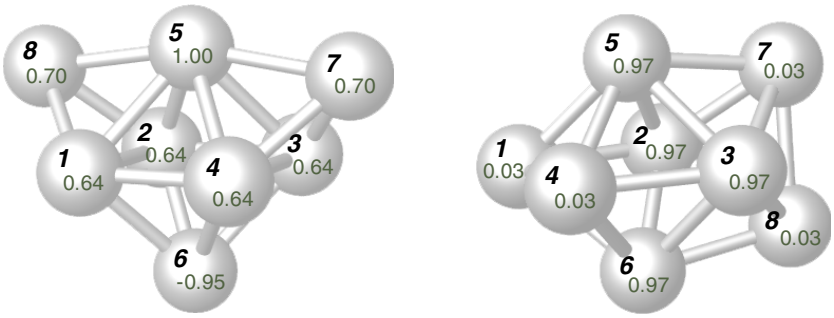

Figure 6. Structure and local magnetic moments of two energetically almost degenerate geometric configurations of Ni_8 clusters in their $S = 4$ ground state: bicapped octahedron (left) and bidisphenoid (right); cf text.

8 meV/atom lower in energy, and does not produce any new configuration. Both nearly degenerate geometry configurations adopt a $S = 4$ (spin-nonet) state; the symmetry is C_{2v} (see figure 6). For configuration 8b, the structure can also be described as slightly distorted bidisphenoid (the undistorted structure would have a higher D_{2d} symmetry). Our prediction agrees with Desmarais *et al* [81]. In their studies additional geometries (cube, square antiprism, capped pentagonal bipyramid) have also been examined which, however, do not correspond to locally stable energy minima. The Ni_8 cluster is one of the largest clusters for which quantum chemical studies of the magnetic ground state have been performed, with conflicting results at different levels of theory (see table 1).

For the Ni_8 cluster we note interesting correlations between the magnetic and geometric structures of the spin isomers. Figure 7 presents the magnetization densities for the $S = 0$–5 states of configuration 8b. For $S = 0$–3 we find an appreciable antiferromagnetic component in the magnetization densities. For the $S = 0$–2 isomers the geometric symmetry is S_4. For $S = 0$ the inversion also induces a reversal of the direction of the magnetic moment, but not for $S = 1$ and 2. For the $S = 2$ state, four Ni moments have nearly zero moment, but the magnetization

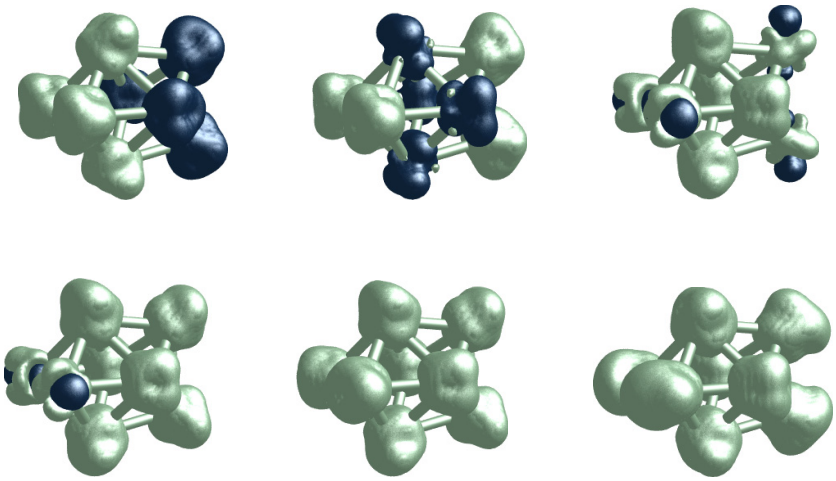

Figure 7. Isosurface plots of the magnetization densities for configuration 8b (bidisphenoid or bicapped octahedron) of the Ni_8 cluster, for $S = 0$–5. Light surfaces represent positive, dark surfaces negative magnetization densities. Note the antiferromagnetic, respectively ferrimagnetic character of the low-spin isomers. Cf text.

densities show that this results from the occupation of two spin-uncompensated eigenstates by electrons with different spins. For $S = 3$, the point-group symmetry is reduced to C_{2v} because the pairs of Ni atoms at the outer edges of the cluster are now magnetically inequivalent (see also the magnetization densities) and magnetostructural effects induce a geometric distortion (the distance between the nearly nonmagnetic atoms 1 and 4 is only 2.27 Å, whereas the distance between atoms 7 and 8 with large magnetic moments is 2.48 Å). For the stable $S = 4$ isomer, the magnetic inequivalence between these two pairs of atoms has nearly disappeared, but the structural distortion still persists. Only for the high-spin ($S = 5$) isomer, the higher S_4 symmetry is recovered. Magnetic energy differences relative to the low-spin isomers are modest; hence complex spin fluctuations are to be expected at finite temperatures.

Our structural predictions for the Ni_N clusters with $N = 6$–8 agree well with the interpretation of the N_2-uptake experiments, with the octahedron presenting the constituent element of the cluster structure. All clusters have a total magnetic moment of $8\mu_B$—this is consistently below the result of the Stern–Gerlach experiments, but agrees with earlier LSDA studies and the recent work of Duan *et al* [91].

3.3. Ni_N clusters, $N = 9$–11—polytetrahedral structures

For clusters of this size, the structures suggested on the basis of the uptake experiments ($N = 9$—bicapped pentagonal bipyramid, $N = 10$—tricapped pentagonal bipyramid, $N = 11$—?) [4] must be considered as a tentative interpretation rather than conclusive results. A number of classical simulations based on various force-field models have been performed (see, e.g., Grigoryan and Springborg [99], Luo [97, 98] and further references given therein), but no *ab initio* structural studies for clusters in this range have been published. The classical simulations lead to structures following a pentagonal growth sequence leading to the 13-atom icosahedron.

3.3.1. Ni_9. For the Ni_9 cluster our calculations have identified two nearly degenerate geometric and magnetic ($S = 4$) configurations: a bicapped pentagonal bipyramid and a double

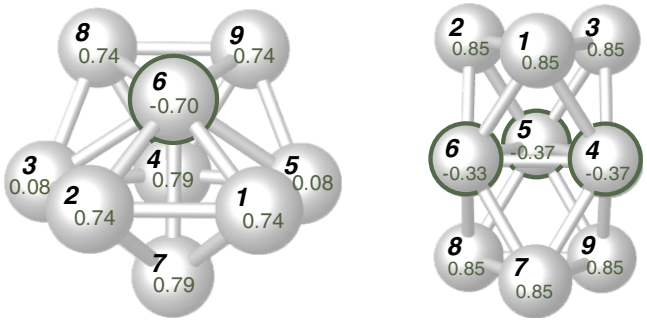

Figure 8. Structure and local magnetic moments of two energetically almost degenerate geometric configurations of Ni_9 clusters in their $S = 4$ ground state: bicapped pentagonal bipyramid (PGS C_{1h}—left) and double trigonal antiprism (PGS D_{3h}—right); cf text.

trigonal antiprism which is only 3 meV/atom higher in energy. The former structure may be considered as a polytetrahedral packing: for the capped pentagonal bipyramid, five slightly distorted tetrahedra are packed around a fivefold axis; three more tetrahedra are added by the capping atoms. In contrast the double antiprism is a polyoctahedral arrangement: two distorted octahedra share a triangular facet. Qualitatively, this agrees with the experimentally suggested structure, but for both configurations, the symmetry is reduced compared to ideal geometry. For all magnetic isomers of the bicapped pentagonal biprism, the point-group symmetry is only C_{1h}, with a mirror plane through the central axis of the bipyramid. In its magnetic ground state the double trigonal bipyramid conserves a higher D_{3h} symmetry (see figure 8).

Both structural isomers show an antiferromagnetic component in the magnetization densities for all isomers up to $S = 3$ (for details, see supporting material available at stacks.iop.org/JPhysCM/18/9703). The result that the ground state of the Ni_9 cluster is ferrimagnetic is indeed remarkable. For the double trigonal antiprism, the magnetic moments of the $S = 1$ and 3 isomers break the D_{3h} symmetry and also induce a weak structural distortion.

3.3.2. Ni_{10}. For the Ni_{10} cluster, our simulations have identified three locally stable configurations: a tetragonal antiprism with capped square basal plane (point-group symmetry C_{4v}—configuration 10a), a double octahedron sharing a common edge (D_{2h}—10b), and a tetrahedron (or trigonal pyramid) with atoms at vertex and mid-edge positions (10c). This last configuration represents the ground state by substantial structural energy differences of 64 and 73 meV/atom, respectively. This is a rather surprising result—our dynamical simulated annealing studies of Pd and Rh clusters had shown that the trigonal pyramid is a metastable configuration, but the strong preference for this structure for the Ni_{10} cluster is still rather unexpected. The symmetry of the trigonal pyramid is closely coupled with the magnetic state: the antiferromagnetic $S = 0$ state has C_{2v} symmetry (see figure 9); for the ferrimagnetic states with $S = 1$–3 the point-group symmetry is reduced to C_{1h}, while the magnetic ground state with $S = 4$ shows tetrahedral symmetry (point group T). All interatomic distances along the edges are 2.27 Å, all distances between atoms in mid-edge positions are 2.41 Å; magnetic moments on vertex on mid-edge sites are $0.74\mu_B$ and $0.84\mu_B$, respectively. Magnetization densities show that eigenstates are spin polarized also on sites with low or zero magnetic moment—for details see the isosurface plots in the supporting material available at stacks.iop.org/JPhysCM/18/9703.

3.3.3. Ni_{11}. For the 11-atom cluster we find the same locally stable configurations as for the Pd_{11} cluster. One consists of two distorted edge-sharing octahedra plus a bridging adatom

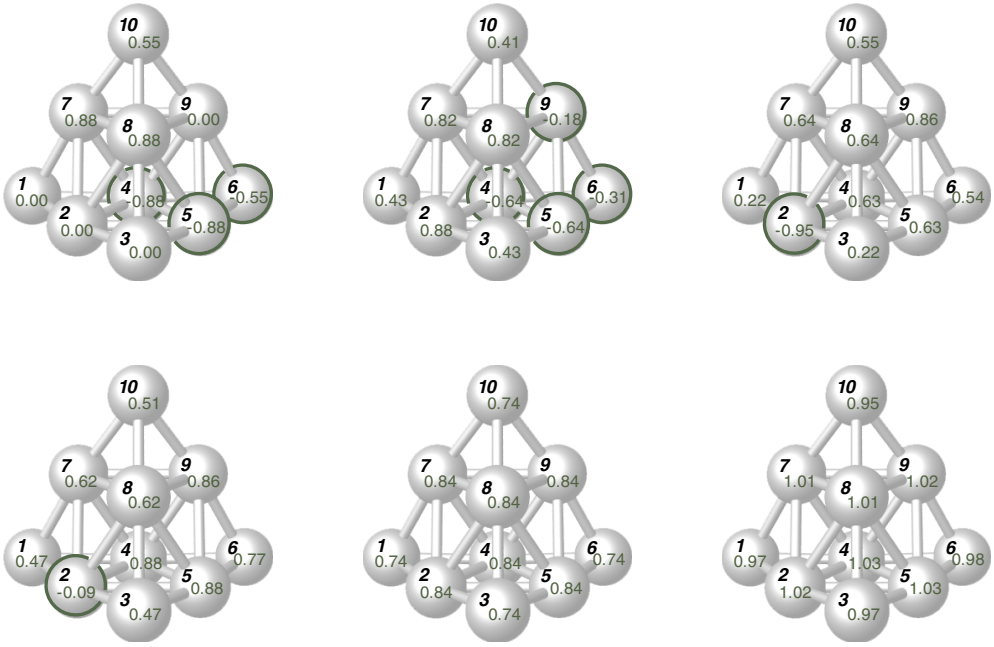

Figure 9. Structure and local magnetic moments of the magnetic isomers of Ni_{10} clusters forming a distorted tetrahedron: $S = 0$—point-group symmetry C_{2v}, $S = 1$–3—C_{1h}, $S = 4$—T, $S = 5$—C_{1h}; cf text.

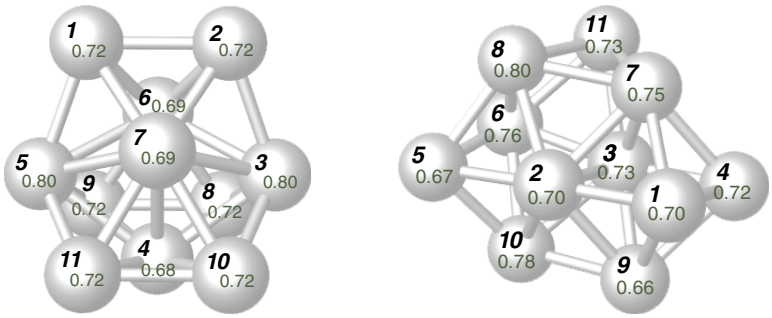

Figure 10. Structure and local magnetic moments of Ni_{11} clusters in configurations 11a (polytetrahedral cluster—left) and 11b (octahedral cluster—right); cf text.

(configuration 11b, point-group symmetry C_1), the second is a complex polytetrahedral cluster (configuration 11a—point-group symmetry C_{2v})—this structure is favoured by an energy difference of 44 meV/atom. Both structures are shown in figure 10: the stable magnetic isomer is $S = 4$ in both cases. For the low-spin isomers we find a strong antiferromagnetic component; details are given in the supporting material available at stacks.iop.org/JPhysCM/18/9703.

3.3.4. Cluster structures—comparison with experiment. The N_2-adsorption experiments for Ni_9 and Ni_{10} clusters have been interpreted in terms of bicapped and tricapped pentagonal antiprisms [71], but no definite structure could be assigned to the Ni_{11} cluster. The proposed structures are based on the idea that already for the Ni_N clusters with $N = 9, 10, 11$ the

pentagonal motif dominant in the icosahedral structure is the constituent element of the cluster structure.

Evidently, our optimizations lead to quite different cluster structures. Hence it is appropriate to rediscuss the rationale behind the structural assignments. The $(N_2)_m$ uptake spectra [71] show a plateau at $m = N - 1$; the plots for CO uptake [72, 73] show plateaus at $m = 15, 17$ for $N = 9$, $m = 16, 18$ for $N = 10$, and $m = 18$–19 for $N = 11$. On Ni surfaces N_2 adsorbs in on-top positions, but it is very weakly bound. Hence the first plateau in the N_2 adsorption plots determines the number of Ni sites exposed on the surface of the cluster and capable of binding a N_2 molecule. CO preferentially adsorbs in hollow sites of Ni surfaces [138]; hence the number of adsorbed CO molecules counts the number of facets on the cluster surface.

For clusters of this size, all atoms are located at the surface; hence to explain the existence of the $m = N - 1$ plateau for N_2 adsorption, one has to look for differences in the coordination that might explain that one atom does not bind a nitrogen molecule. Of the two structural isomers of the Ni_9 cluster, all atoms of the capped pentagonal biprism have coordination number 4 or 5, except atoms 6 with $N_C = 7$ and 4 with $N_C = 6$. On the double trigonal antiprism, six atoms have $N_C = 4$ and three atoms $N_C = 6$. As the most highly coordinated site binds a molecule most weakly, the former structure is compatible with the $m = N - 1$ plateau, while the latter is not. This agrees with our structural energy difference (which is, however, only minimal). For the Ni_{10} cluster, the local coordination is quite homogeneous for all three isomers, none of which offers an explanation for the $m = N - 1$ plateau. For both isomers of the $N = 11$ cluster, there is just one site with the maximal coordination number 8 (atom 4 for the polytetrahedral cluster, atom 3 for the octahedral cluster; see figure 10); hence N_2 adsorption cannot discriminate between these two structures.

For the interpretation of the CO-uptake experiments, the situation is similar. For the Ni_9 cluster both locally stable structures have 14 triangular facets; hence interpretation of the observed plateaus requires adsorption of more than one molecule on one or three facets. For the Ni_{10} structure, all three structural variants have 16 triangular facets; hence the $m = 16$ plateau for CO is compatible with all three structures. For the N_{11} cluster, the polytetrahedral configuration 11a offers 18 triangular facets, the polyoctahedral configuration 11b only 17. Hence the CO-adsorption analysis agrees with our prediction of a minimum energy for the former.

For clusters of this size, the Stern–Gerlach experiments find large magnetic moments ranging from $1.55\mu_B$/atom for $N = 8$ to $1.2\mu_B$ for $N = 11$. All available DFT calculations [87, 91] agree with our result of a stable $S = 4$ state for all clusters, i.e. a magnetic moment decreasing from $1\mu_B$ to $0.73\mu_B$. Only the semiempirical calculations [95, 96] lead to magnetic moments in almost perfect agreement with experiment.

3.4. Ni_N clusters, $N = 12, 13$—icosahedra

For clusters of this size, experiments and classical simulations agree on an icosahedral structure (icosahedron with a vacant surface site for $N = 12$), while our previous studies of Pd_N and Rh_N (see I) and the work of Chang and Chou [65] on a series of 4d-metal clusters predicted the icosahedron to be less stable than a polyoctahedral structure.

3.4.1. Ni_{12}. For a cluster of 12 Ni atoms, we found four at least metastable structural configurations: (a) a distorted cube with four capped faces, (b) an incomplete icosahedron with a vacant surface site, (c) a polyoctahedral cluster, and (d) a pyramid with a basis in the form of a buckled centred hexagon, topped by a square pyramid; see figure 11. The

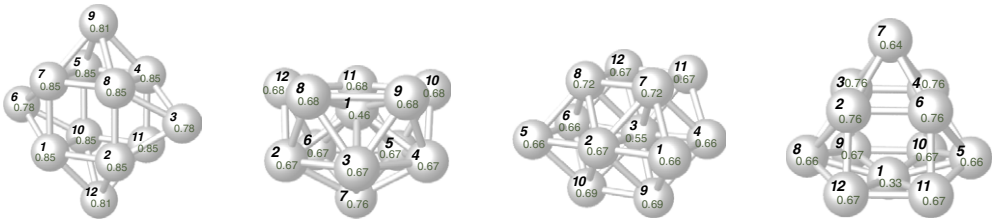

Figure 11. Structure and local magnetic moments of Ni_{12} clusters in its four metastable configurations (from left to right): capped cube—point group symmetry D_{4h}; $S = 5$, incomplete icosahedron—C_{5v}, $S = 4$; polyoctahedral cluster—C_{1h}, $S = 4$; pyramid—C_{2v}, $S = 4$; cf text.

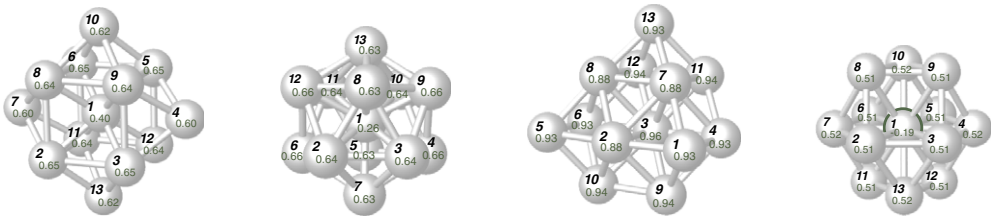

Figure 12. Structure and local magnetic moments of Ni_{13} clusters in its four metastable configurations (from left to right): capped cube—point-group symmetry D_{2h}; $S = 5$, icosahedron—C_{1h}, $S = 4$; polyoctahedral cluster—C_{1h}, $S = 6$; cuboctahedron—C_{2v}, $S = 3$; cf text.

icosahedron with $S = 4$ has the lowest energy, but is only 10 meV/atom lower in energy than configuration (d).

For most magnetic isomers of the incomplete icosahedron, the point-group symmetry is reduced to C_{1h}, and the magnetization density of the low-spin isomers up to $S = 3$ shows a strong ferrimagnetic component. For the stable $S = 4$ isomer, the full pentagonal symmetry of both the geometric and the magnetic structures (C_{5v}) is recovered. It is again reduced to C_{1h} if the spin state is enhanced to $S = 10$. The polyoctahedral cluster representing the ground-state configuration of the homologous Pd_{13} and Pt_{13} clusters is 31 meV/atom higher in energy. Configuration (d) resulted from a dynamical simulated annealing run. Like for the incomplete icosahedron, the symmetry is reduced to C_{1h} for the low-spin states, while for the stable $S = 4$ isomer a more symmetric configuration (C_{2v}) is stabilized.

The CO-uptake experiments for the Ni_{12} cluster show three plateaus at $m = 18, 20, 22$. The incomplete icosahedron has 20 triangular facets—this corresponds to the second plateau in the uptake plots. The first could result from a lower occupancy of the concave side of the cluster. The three metastable structural isomers have between 12 (conf. a) and 15 (conf. c) triangular facets and one or two square facets, which is difficult to reconcile with the uptake experiments.

3.4.2. Ni_{13}. For the Ni_{13} cluster all force-field simulations and DFT calculations published so far predict an icosahedral geometry. Quantum-chemical calculations agree with this result at the UHF level [78], whereas MRCI calculations find an octahedral symmetry to lead to a lower energy. We have identified four locally stable structural isomers (see figure 12): (a) a capped centred cube, (b) the icosahedron, (c) a cluster of three octahedra, corresponding to the 'buckled biplanar' structure forming the ground state of Pd_{13}, and (d) a cuboctahedron. All structures are distorted from the ideal geometry. The icosahedron is the ground state; it

is 31 meV/atom lower in energy that the cluster of octahedra. The stable magnetic isomers varies from one structure to the other: the magnetic moment is lowest for the cuboctahedron ($S = 3$), and the ground state of the icosahedron is a spin nonet ($S = 4$, like all Ni clusters from $N = 6$ to 13), while the cluster of octahedra ($S = 6$) and the capped cube ($S = 5$) have larger magnetic moments.

The I_h symmetry of the Ni_{13} icosahedron is broken—this is evident from the cluster geometry, and even more so from the local magnetic moments (see figure 13). In the spin-singlet state, the Ni_{13} cluster is antiferromagnetic with local magnetic moments varying between $-0.59\mu_B$ and $+0.64\mu_B$; the point-group symmetry is reduced to C_{1h}, with distances between the centre and the vertices varying between 2.31 and 2.34 Å, and distances between the vertices varying between 2.38 and 2.48 Å (details are given in the supporting material available at stacks.iop.org/JPhysCM/18/9703). The magnetization densities on all vertices are of mixed spin-up/spin-down character. Spin isomers with $S = 1$–3 are ferrimagnetic, with a negative moment on the centre of the icosahedron and varying positive magnetic moments on the surface atoms. The distortions from icosahedral symmetry are gradually reduced with increasing spin. For $S = 1$, only the central atom and two atoms occupying opposite vertices are strongly magnetic; on all other site the local moment is $\leqslant 0.1\mu_B$. The $S = 2$ isomer has almost I_h symmetry: all distances from the centre to the surface atoms are ∼2.32 Å, distances between the surface atoms are 2.44 ± 0.01 Å. The central atom has a magnetic moment of $-0.57\mu_B$; atoms on the surface have $+0.38 \pm 0.01\mu_B$. The geometry distortions are similar for the $S = 3$ isomer, but the local magnetic moments strongly violate icosahedral symmetry. For the stable magnetic isomer ($S = 4$), all surface atoms carry bulk-like magnetic moments (0.63–$0.66\mu_B$), but differences in the centre-to-vertex distances of up to 0.04 Å show that the icosahedral point-group symmetry is broken, it is reduced to C_{1h}. The structural distortions are even more pronounced for the $S = 5$ isomer, with difference of up to 0.13 Å in the centre–vertex distances. Magnetic energy differences are relatively large, at least 24 meV/atom.

Similar magnetostructural effects are found also in the other isomers; they are most pronounced for the cuboctahedron. Here the point-group symmetry is D_{3h} for the $S = 0$ state; it decreases to C_{2v} for $S = 1, 2$, and increases to almost perfect O_h symmetry for the stable $S = 3$ isomer. For higher spin, both the geometric and the magnetic symmetry are again reduced. For all metastable structures, magnetic energy differences are very small.

3.5. Ni clusters—trends in structure and magnetic moments

Our search for the optimum structure of Ni clusters reveals some interesting trends: (i) the stable structures of the Ni_4 and Ni_5 clusters are a distorted tetrahedron (symmetry S_4) and a distorted trigonal bipyramid (symmetry D_{3h}); in both cases the symmetry breaking is most pronounced for the low-spin isomers. (ii) The structures for clusters with 6, 7, and 8 atoms are based on distorted a octahedron plus adatom(s), with point-group symmetries D_{4h}, C_{3v}, and C_{2v}, respectively. Again symmetry and magnetic moments are strongly linked. (iii) The structures for clusters with 9–13 atoms are essentially based on a polytetrahedral packing, beginning with the capped pentagonal bipyramid for Ni_9 (five distorted tetrahedra packed around a central axis, plus two more tetrahedra created by two adatoms, symmetry C_{1h}). The Ni_{10} cluster forms a tetrahedron with atoms at the vertices and mid-edge positions; only the magnetic ground state has full tetrahedral (T) symmetry. Ni_{11} forms a polytetrahedral cluster created by adding 2×2 atoms to a pentagonal bipyramid. The structures of the Ni_{12} and Ni_{13} clusters are based on the icosahedron, with one vacant site for the 12-atom cluster. Interestingly, the magnetic ground state of the incomplete icosahedron shows full pentagonal symmetry (C_{5v}) while none of the magnetic isomers of Ni_{13} shows full icosahedral symmetry. The smallest distortions occur for

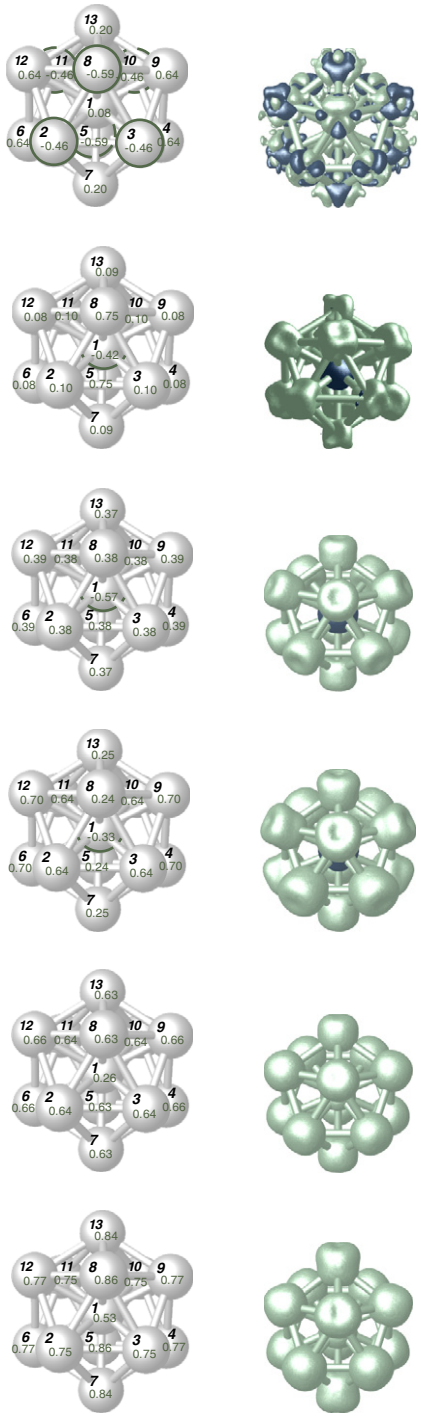

Figure 13. Local magnetic moments (left column) and isosurface plots of the magnetization densities of Ni_{13} forming a distorted icosahedron, for $S = 0$ (top) to $S = 5$ (bottom). Cf text.

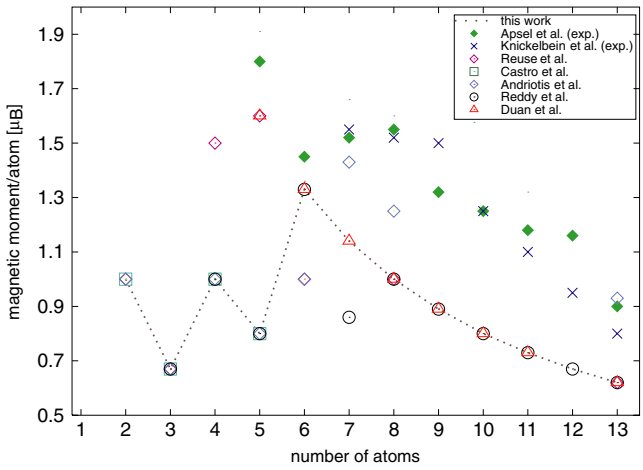

Figure 14. Magnetic moments per atom (in μ_B) for Ni clusters as a function of cluster size.

the $S = 2$ state, while the magnetic ground state has $S = 4$. The structures for these larger Ni clusters differ from those of the Pd clusters which are based on polyoctahedral motifs.

Figure 14 shows the calculated magnetic moments of the Ni clusters as a function of size, together with the available experimental data [51, 53] and other calculations based on DFT and TB methods. In the range where experimental moments are available, all DFT calculations produce substantially lower magnetic moments than those measured experimentally. For $N \geqslant 6$ the present calculations and those of Duan *et al* [91] and Reddy *et al* [87] (with the exception of $N = 7$) predict a constant total moment of $M = 8\mu_B$—this is remarkable since the calculations are based on different functionals (GGA, LSDA) and also different cluster structures. In this range, the semiempirical TB calculations of Aguilera-Granja *et al* [95] and Hernandez *et al* [96] produce almost perfect agreement with the experimental data—this underlines the success of the parameterization, but is certainly not an expression of the predictive power of TB techniques. For smaller clusters, even smaller magnetic moments are found; our present work agrees with the previous DFT calculations of Castro *et al* [83] and Reddy *et al* [87], while there are certain discrepancies with the work of Reuse *et al* [79–82]. Interestingly, for $N \leqslant 5$, the TB results of Andriotis *et al* [93] agree perfectly with DFT, while for $N = 7, 8$, TB produces again larger moments.

Guirado-Lopez *et al* [139] have argued that the discrepancy between DFT and experiment is due to a large orbital moment in the clusters, and that the contribution of the orbital moment is particularly important for Ni where the difference between the orbital moment of the free atom ($L = 2\mu_B$ for an electron configuration d^9s^1) and in the bulk ($L = 0.05\mu_B$) is rather dramatic. The analysis is based on a Hamiltonian including a one-electron tight-binding term, on-site Coulomb repulsion and exchange are treated in the unrestricted Hartree–Fock approximation (with an on-site Coulomb-repulsion of $U = 9.5$ eV and an exchange potential of $J = 0.5$ eV for Ni-d electrons), and a spin–orbit coupling term. An orbital moment of $L \sim 0.3$–$0.4\mu_B$ for clusters with 3–13 atom results from three main effects. (i) The strong on-site Coulomb repulsion favours the occupation of states with high angular momentum. (ii) The reduced coordination in the small clusters induces an enhanced spin moment, which induces in turn larger orbital moments via the spin–orbit coupling. (iii) Degeneracies in the one-electron spectrum lead to a more effective spin–orbit coupling even in cases where the spin moment is nearly saturated (i.e. close to the limiting value imposed by Hund's rule).

Very recently, a similar study based on a tight-binding Hamiltonian plus spin–orbit and on-site Hubbard corrections has been presented by Wan *et al* [140]. Using values of $U = 2.6$ eV and $J = 1.1$ eV, an orbital moment linearly decreasing from $L = 1\mu_B$ for $N = 9$ to $L = 0.2\mu_B$ for $N = 13$ (and fluctuating around $L \sim 0.4\mu_B$ for larger clusters with $N \leqslant 60$) was reported. The orbital moment was shown to depend quite strongly on the value of U, so it is hard to understand that with a rather modest value of U even larger orbital moments than in the study by Guirardo-Lopez *et al* [139] are reported. Hence at the moment the evidence for a large orbital magnetic moment is only qualitative and should be backed by fully relativistic *ab initio* calculations.

4. Geometric and magnetic structures of Pt_N clusters

Our results for the structural and magnetic isomers of Pt_N clusters are summarized in table 3; extensive information on all structures, interatomic distances and local magnetic moments is compiled in the supporting material to be found at stacks.iop.org/JPhysCM/18/9703 and on our website. Among previous theoretical studies of Pt clusters [104–116], large discrepancies concerning the geometric and magnetic structures of the ground-state configurations exist.

4.1. Pt_N, $N = 2$–6*: from planar to three-dimensional structures*

For the smallest Pt clusters, there is still an open controversy whether Pt clusters with four to six atoms adopt planar or three-dimensional configurations. Yang *et al* [104] performed non-selfconsistent DFT calculations based on the Harris functional and predicted all clusters of this size to be planar. Grönbeck and Andreoni [106] also found that for a Pt tetramer a flat rhombus has a lower energy than a distorted tetrahedron, but for the pentamer they obtained a lower energy for a square pyramid at the LDA level, while a calculation with a gradient-corrected functional predicts a planar configuration. Lin *et al* [107] found a tetrahedral structure for the Pt_4 cluster, and Li and Balbuena [108] predicted a tetrahedron, a square pyramid, and a trigonal bipyramid to be the equilibrium structures for Pt_4, Pt_5 and Pt_6 clusters, respectively. The result for Pt_5 also agrees with the quantum-chemical calculations of Majumdar *et al* [116], who found a distorted bipyramidal structure. In addition, there is widespread disagreement on the spin of the ground state. Whereas Lin *et al* [107] found $S = 0, 1, 2$ for $N = 2, 3, 4$, Li and Balbuena [108] report $S = 1, 1, 2$ for $N = 4, 5, 6$, while Grönbeck and Andreoni [106] found that LDA and GGA calculations lead to different predictions for the magnetic moment, with GGA preferring a higher spin.

4.1.1. Pt_2. The ground state of the Pt dimer is a triplet state ($S = 1$) with a bond length of 2.33 Å and a modest binding energy of 1.49 eV/atom. The calculated bond length agrees with the GGA result of Xiao and Wang [113], while a quantum-chemical approach at the complete active space SCF (CASSCF) level, followed by first-order configuration interaction calculations [141] produces bond lengths in the range of 2.4–2.6 Å for the lowest-lying electronic states, i.e. still much shorter than the equilibrium interatomic distance in bulk Pt of 2.77 Å. The calculated bond length and binding energy agrees very well with the experimental values [142, 143] of 2.34 Å and 1.57 eV/atom.

4.1.2. Pt_3. For the Pt trimer the ground-state configuration consists of an equilateral triangle (point-group symmetry D_{3h}) in the spin-triplet state, a bond length of 2.49 Å and a binding energy of 2.06 eV/atom. The calculated bond length is in good agreement with previous DFT calculations at the GGA level [107, 113, 144], but there is some disagreement on the magnetic ground state. Lin *et al* [107] also find a triplet state, whereas Xiao and Wang [113] find the

Table 3. Point-group symmetry (PGS), total magnetic moment M (in μ_B, magnetic order O (NM—nonmagnetic, AF—antiferromagnetic, FI ferrimagnetic, otherwise ferromagnetic), average coordination number N_C, average nearest-neighbour distance d (in Å), HOMO–LUMO gap E_g (in eV), and binding energy (in eV/atom) for structural and magnetic isomers of Pt_N clusters with $N = 2$–13. The last two columns list the magnetic energy differences ΔE_{mag} for each structural isomer, and the structural energy difference ΔE_{struct} (both in meV/atom) calculated for the respective magnetic ground state. An asterisk added to the PGS symbol indicates that the magnetic symmetry of the cluster is reduced.

N	Structure	PGS	M	O	N_C	d	E_g	Binding energy	ΔE_{mag}	ΔE_{struct}
2	Dimer	$D_{\infty h}$	0	NM	1	2.34	0.1007	1.316	176	
		$D_{\infty h}$	2		1	2.33	0.2688	1.492	—	
		$D_{\infty h}$	4		1	2.32	0.3760	1.047	445	
3	Triangle	D_{3h}	0	NM	2	2.47	0.1342	2.049	14	
		D_{3h}	2		2	2.49	0.1139	2.063	—	
		C_{2v}	4		2	2.50	0.3407	1.814	250	
4a	Square	D_{4h}	0	NM	2	2.45	0.0989	2.281	26	
		D_{4h}	2		2	2.47	0.1342	2.304	3	
		D_{4h}	4		2	2.45	0.2258	2.307	—	39
4b	Rhombus	D_{2h}	0	NM	2.5	2.50	0.0989	2.281	66	
		D_{2h}	2		2.5	2.52	0.1771	2.324	23	
		D_{2h}	4		2.5	2.52	0.2209	2.346	—	2
4c	Tetrahedron	C_{2v}	0	AF	3	2.60	0.1935	2.330	18	
		C_{2v}	2		3	2.60	0.1858	2.348	—	—
		S_4	4		3	2.58	0.0000	2.326	22	
5a	Square pyramid	C_{4v}	0	AF	3.2	2.59	0.4053	2.547	12	
		C_{4v}	2	FI	3.2	2.60	0.2053	2.539	20	
		C_{4v}	4		3.2	2.59	0.0000	2.524	34	
		C_{4v}	6		3.2	2.58	0.1065	2.559	—	35
5b	Trigonal bipyramid	D_{3h}	0	AF	3.6	2.62	0.0000	2.473	120	
		D_{3h}	2		3.6	2.61	0.3307	2.560	34	
		D_{3h}	4		3.6	2.61	0.3869	2.593	—	—
		D_{3h}	6		3.6	2.61	0.0000	2.485	108	
5c	Flat trigonal bipyramid	D_{3h}	0	AF	2.8	2.58	0.0000	2.397	53	
		D_{3h}	2		2.8	2.59	0.5473	2.450	—	144
		D_{3h}	4		2.8	2.57	0.0000	2.415	35	
		D_{3h}	6		2.8	2.55	0.3809	2.414	36	
6b	Octahedron	O_h	0	NM	4	2.65	0.1577	2.672	48	
		D_{4h}	2	FI	4	2.64	0.2436	2.678	41	
		O_h^*	4		4	2.62		2.685	34	
		O_h^*	6		4	2.62	0.4870	2.719	—	23
		O_h	8		4	2.63	0.0000	2.708	11	
6c	Incomplete PBP	C_{1h}	0	AF	4	2.63	0.2509	2.679	30	
		C_{1h}	2	FI	4	2.64	0.1791	2.683	26	
		C_{2v}	4		4	2.65	0.0991	2.688	21	
		C_{2v}	6		4	2.64	0.2210	2.709	—	34
6d	Square pyramid plus adatom	C_{1h}	0	AF	3.7	2.61	0.1750	2.701	41	
		C_{1h}	2		3.7	2.61	0.1521	2.730	13	
		C_{1h}	4		3.7	2.61	0.0896	2.735	8	
		C_{1h}	6		3.7	2.61	0.1372	2.743	—	—
		C_{1h}	8		3.7	2.60	0.1674	2.669	74	
7a	Centred hexagon	D_{2h}	0	NM	3.4	2.55	0.0860	2.746	25	
		D_{2h}	2		3.4	2.55	0.0010	2.757	14	
		D_{2h}	4		3.4	2.56	0.0572	2.762	9	
		D_{2h}	6		3.4	2.57	0.0119	2.771	—	59
		D_{2h}	8		3.4	2.58	0.0000	2.728	43	

Table 3. (Continued.)

N	Structure	PGS	*M*	O	N_C	*d*	E_g	Binding energy	ΔE_{mag}	ΔE_{struct}
7b	Pentagonal Bipyramid	C_{2v}	0	NM	4.6	2.68	0.0000	2.715	115	
		C_{2v}	2		4.6	2.68	0.1404	2.772	57	
		C_{2v}	4		4.6	2.68	0.1103	2.790	39	
		C_{2v}	6		4.6	2.67	0.0894	2.830	—	46
		C_{2v}	8		4.6	2.67	0.1389	2.783	47	
7c	Octahedron	C_1	0	AF	4.3	2.63	0.0613	2.815	61	
	with capped	C_{1h}	2	FI	4.3	2.65	0.1608	2.852	24	
	triangular face	C_{1h}	4		4.3	2.65	0.1181	2.838	38	
		C_{1h}	6		4.3	2.63	0.0610	2.863	13	
		C_{1h}	8		4.3	2.64	0.0610	2.876	—	—
		C_{3v}	10		4.3	2.64	0.3488	2.715	162	
8a	Bicapped octahedron I	C_{2v}	0	AF	4.5	2.66	0.0791	2.970	49	
		C_{2v}	2	FI	4.5	2.66	0.0000	2.976	44	
		C_{2v}	4		4.5	2.65	0.1520	3.000	20	
		C_{2v}	6		4.5	2.65	0.0965	3.009	10	
		C_{2v}	8		4.5	2.65	0.0462	3.020	—	—
		C_{2v}	10		4.5	2.65	0.2899	2.880	140	
8b	Bicapped octahedron II	S_4	0	NM	4.5	2.65	0.1103	2.940	40	
	(Bidisphenoid)	S_4	2	FI	4.5	2.65	0.1228	2.953	28	
		S_4	4	FI	4.5	2.65	0.1302	2.950	31	
		C_{2v}	6		4.5	2.65	0.0872	2.956	24	
		C_{2v}	8		4.5	2.66	0.1037	2.980	—	39
		S_4	10		4.5	2.66	0.0518	2.950	30	
9a	Capped pentagonal	C_{1h}	2	FI	4.9	2.69	0.0357	3.061	26	
	bipyramid	C_{1h}	4	FI	5.1	2.70	0.0190	3.065	22	
		C_{1h}	6		4.7	2.67	0.1496	3.080	6	
		C_{1h}	8		4.7	2.67	0.2128	3.087	—	37
		C_{1h}	10		4.2	2.63	0.0940	3.005	82	
9b	Double trigonal antiprism	D_{3h}	0	NM	4.7	2.64	0.1925	3.068	56	
		D_{3h}	2	FI	4.7	2.64	0.1963	3.097	28	
		D_{3h}	4		4.7	2.65	0.1208	3.105	20	
		C_{2v}	6		4.7	2.65	0.0862	3.124	—	—
		D_{3h}	8		4.7	2.65	0.1419	3.117	7	
		D_{3h}	10		4.7	2.66	0.4519	3.031	93	
10a	Trigonal antiprism	C_{4v}	0	NM	4.8	2.64	0.0508	3.066	54	
	with capped square faces	C_{4v}	2	FI	4.8	2.65	0.0575	3.081	38	
		C_{4v}	4		4.8	2.65	0.1328	3.095	24	
		C_{4v}	6		4.8	2.65	0.1141	3.115	5	
		C_{4v}	8		4.8	2.66	0.0927	3.120	—	245
		C_{4v}	10		4.8	2.66	0.1182	3.107	13	
10b	Edge-sharing	D_{2h}	0	NM	5	2.67	0.1030	3.140	15	
	double octahedra	D_{2h}	2		5	2.66	0.0502	3.144	11	
		D_{2h}	4		5	2.67	0.0427	3.148	7	
		D_{2h}	6		5	2.67	0.0327	3.148	8	
		D_{2h}	8		5	2.66	0.0291	3.155	—	210
		D_{2h}	10		5	2.66	0.0560	3.114	42	
10c	Tetrahedron	C_{1h}	0	AF	4.8	2.66	0.0651	3.311	54	
		C_{1h}	2	FI	4.8	2.66	0.0377	3.322	43	
		T*	4		4.8	2.66	0.0658	3.332	33	
		T*	6		4.8	2.66	0.4757	3.344	22	
		T	8		4.8	2.66	0.4464	3.365	—	—
		C_{3v}	10		4.8	2.66	0.3098	3.224	141	

Table 3. (Continued.)

N	Structure	PGS	M	O	N_C	d	E_g	Binding energy	ΔE_{mag}	ΔE_{struct}
11a	Polytetrahedral	C_{2v}	0	AF	4.3	2.64	0.0003	3.334	12	
	cluster	C_{2v}	2		4.3	2.64	0.2982	3.346	—	1
		C_{2v}	4		4	2.62	0.0685	3.324	22	
		C_{2v}	6		3.8	2.61	0.1319	3.309	37	
		C_{2v}	8		5.5	2.70	0.1466	3.299	47	
11c	Pyramid	C_{2v}	0	NM	4.2	2.61	0.1488	3.341	6	
		C_{2v}	2	FI	4.2	2.61	0.1663	3.347	—	—
		C_{2v}	4		4.2	2.61	0.0935	3.336	11	
		C_{2v}	6		4.2	2.61	0.0184	3.323	23	
		C_{2v}	8		4.2	2.62	0.0621	3.303	44	
12a	Capped cube	D_{4h}	0	NM	4.7	2.62	0.1094	3.343	7	
		D_{4h}	2		4.7	2.63	0.2009	3.348	2	
		D_{4h}	4		4.7	2.63	0.0370	3.350	—	40
		D_{4h}	6		4.7	2.63	0.0825	3.331	19	
		C_{2h}	8		4.7	2.64	0.0248	3.310	40	
12c	Edge-sharing octahedra	C_{1h}	0	AF	5	2.66	0.0388	3.298	13	
	plus two adatoms	C_1	2	FI	5	2.67	0.0133	3.305	5	
		C_{1h}	4		5	2.67	0.0298	3.306	5	
		C_{1h}	6		5	2.67	0.0899	3.311	—	80
		C_{1h}	8		5	2.68	0.0996	3.300	11	
12d	Pyramid	C_{2v}	0	NM	4.7	2.63	0.0428	3.381	9	
		C_{2v}	2		4.7	2.63	0.1090	3.390	—	—
		C_{2v}	4		4.7	2.63	0.0329	3.377	17	
		C_{2v}	6		4.7	2.63	0.1043	3.372	27	
		C_{2v}	8		4.7	2.64	0.1213	3.348	41	
13a	Capped cube	D_{4h}	0	NM	4.9	2.67	0.0846	3.309	3	
	with central atom	D_{4h}	2		4.9	2.67	0.2776	3.312	—	87
		C_{2v}	4		4.9	2.68	0.0302	3.295	17	
		C_{2v}	6		4.6	2.66	0.1696	3.285	27	
		D_{4h}	8		5.5	2.70	1.3288	3.271	41	
13b	Centred icosahedron	C_{2h}	0	NM	6.5	2.73	0.0418	3.233	7	
		C_{2h}	2		6.5	2.73	0.0587	3.240	—	159
		C_{2h}	4		6.5	2.73	0.0310	3.235	4	
		C_{2h}	6		6.5	2.74	0.0269	3.234	6	
		C_{2h}	8		6.5	2.74	0.0260	3.230	10	
13c	Cluster of octahedra	C_{3v}	0	NM	5.5	2.65	0.1055	3.399	—	—
		C_{3v}	2		5.5	2.66	0.0716	3.397	1	
		C_{1h}	4		5.5	2.66	0.0312	3.385	14	
		C_{1h}	6		5.5	2.65	0.0818	3.381	18	
		C_{1h}	8		5.5	2.66	0.1574	3.373	8	

Pt trimer to be nonmagnetic. Indeed we find that the magnetic energy difference between the $S = 1$ and 0 states is only 14 meV/atom. For the two low-spin isomers, the threefold symmetry is conserved, whereas for the energetically much less favourable $S = 2$ state the symmetry is reduced to C_{2v}.

4.1.3. Pt_4. For the Pt tetramer we find three locally stable structural isomers. A distorted tetrahedron (point group symmetry C_{2v}) is only 2 meV/atom lower in energy than a Pt_4 rhombus with D_{2h} symmetry, but by 39 meV/atom more favourable than a Pt_4 square with

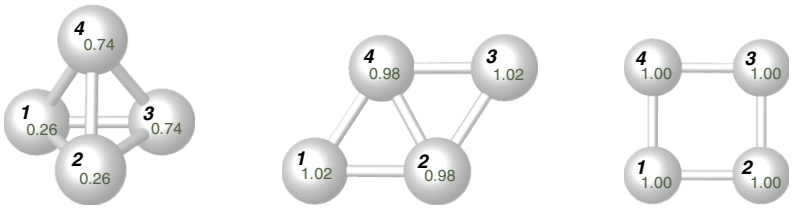

Figure 15. Structure and local magnetic moments of Pt_4 clusters in their three metastable configurations (from left to right): distorted tetrahedron—point group symmetry C_{2v}; $S = 1$; rhombus—D_{2h}, $S = 2$; square—D_{4h}, $S = 2$; cf text.

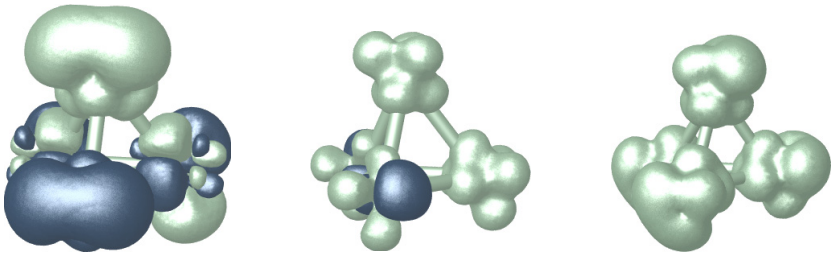

Figure 16. Isosurface plots of the magnetization densities for the three magnetic isomers of a tetrahedral Pt_4 cluster with $S = 0$–2 (from left to right). The point-group symmetry is C_{2v} for the two low-spin isomers and S_4 for the $S = 2$ state; cf text.

full D_{4h} symmetry; see figure 15. The structural stability is the result of a higher average coordination number: $N_C = 3$ for the tetrahedron, $N_C = 2.5$ for the rhombus and $N_C = 2$ for the square. The trend in the bond lengths follows that in the coordination number according to bond-order conservation: $d = 2.45$ Å for the square, $d = 2.51$–2.52 Å for the rhombus, and $d = 2.57$–2.68 Å for the distorted tetrahedron.

The magnetic ground state of the tetrahedron is an $S = 1$ triplet, whereas for the two planar isomers it is an $S = 2$ quintuplet. In the $S = 0$ state, the square and the rhombus are nonmagnetic, whereas the tetrahedron is antiferromagnetic, with large positive and negative moments on one edge, and nonmagnetic atoms on the other edge. However, the analysis of the magnetization densities (see figure 16) shows that the zero local moment results from a simultaneous occupation of spin-up and spin-down orbitals on these sites. In the $S = 1$ ground state, two sites carry large ($0.74\mu_B$) moments, and two sites small ($0.26\mu_B$) moments—again this results from spin-up and spin-down components in the magnetization densities. In the high-spin isomer, all four sites are magnetically equivalent, but the symmetry is only S_4.

The trend in the structural stability (tetrahedron–rhombus–square) and in the interatomic distances agrees qualitatively with Xiao and Wang [113]. However, they find a larger structural energy difference between tetrahedron and rhombus because the possibility of an $S = 2$ state has been ignored.

4.1.4. Pt_5. For the Pt pentamer we have identified three locally stable structural isomers: a square pyramid (symmetry C_{4v}), an acute and a flat trigonal bipyramid (symmetry D_{3h}). The ground-state configuration is the $S = 2$ state of the acute trigonal bipyramid, which is 35 meV/atom lower in energy than the square pyramid and 144 meV/atom lower than the flat trigonal bipyramid. The sequence in the structural stability is again determined by the maximum number of nearest-neighbour bonds. All three structural isomers differ in their

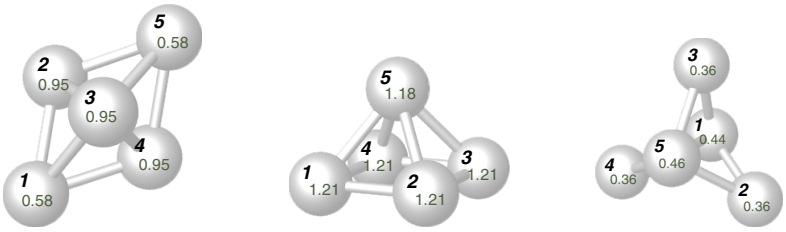

Figure 17. Structure and local magnetic moments of Pt_5 clusters in their three metastable configurations (from left to right): acute trigonal bipyramid—point-group symmetry D_{3h}; $S = 2$; square pyramid—C_{4v}, $S = 3$; flat trigonal bipyramid—D_{3h}, $S = 1$; cf text.

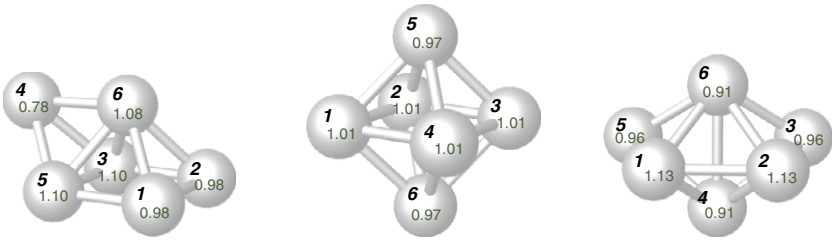

Figure 18. Structure and local magnetic moments of Pt_6 clusters in their three metastable configurations (from left to right): capped square prism—point group symmetry C_{1h}, $S = 3$; octahedron—O_h, $S = 3$—note that the local magnetic moments violate the full octahedral symmetry; incomplete pentagonal bipyramid—C_{1h}, $S = 3$; cf text.

magnetic ground state (see figure 17 for details). The predicted stability of the trigonal bipyramid, magnetic moment and bond lengths (2.53 Å between the atoms forming the central triangle, 2.63 Å to the atoms at the vertices) agree with Xiao and Wang [113], but the planar isomers described by these authors where found to be unstable. Our results are in contradiction to the finding of Yang *et al* [104] and Grönbeck and Andreoni [106] that planar structures are preferred to three-dimensional arrangements, but agree with the DFT results of Fortunelli [105] and the quantum-chemical calculations of Dai *et al* [114–116] in their preference for a three-dimensional structure.

4.1.5. Pt_6. For the Pt_6 cluster the locally stable structural isomers are the octahedron (point group symmetry O_h), an incomplete pentagonal bipyramid (C_{1h}), and a square pyramid plus an adatom capping a triangular facet (C_{1h}); see figure 18—surprisingly the last structure represents the ground state. A pentagonal pyramid is found to be unstable; it transforms spontaneously to the ground-state structure. The magnetic ground state of all three structural isomers is $S = 3$. All three isomers have a strong spin-down component in their magnetization densities; see figure 19 for the stable structural isomer. In the $S = 0$ state, the two triangles forming this structure are coupled antiferromagnetically, and even the magnetic ground state is still relatively inhomogeneous, the smallest and largest magnetic moments being $0.78\mu_B$ and $1.08\mu_B$, respectively (see supporting material for details available at stacks.iop.org/JPhysCM/18/9703). The Pt_6 octahedron is nonmagnetic, with perfect O_h symmetry, in the spin-singlet state. In the $S = 1$ state, the symmetry is reduced to D_{4h}, with negative moments at the axial vertices. For the higher-spin isomers, the O_h symmetry of the geometric structure is nearly recovered but the distribution of the local moments has only fourfold symmetry.

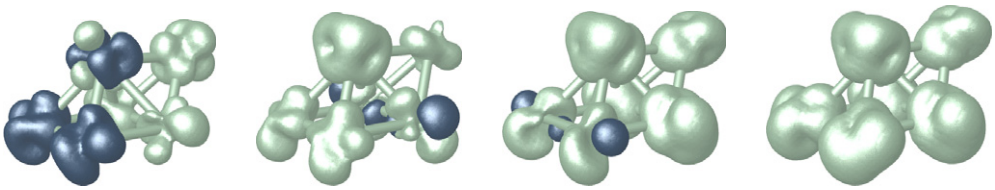

Figure 19. Isosurface plots of the magnetization densities for the four magnetic isomers of a Pt_6 cluster forming a capped square prism with $S = 0$–3 (from left to right).

Previous DFT calculations by Yang *et al* [104] and Xiao and Wang [113] had predicted planar structures for the Pt hexamer. The planar structure identified by the last authors as the ground state consists of a rectangle and two triangles, with nearest-neighbour bonds measuring between 2.41 and 2.79 Å. It is reported to be lower in energy than all other planar and three-dimensional structures (where a trigonal prism is reported to be favoured over the octahedron) by 150 meV/atom, while the structural energy differences between the two three-dimensional isomers and two planar structures are all around 10 meV/atom only. Due to the outstanding difference in the binding energies and too large differences in the nearest-neighbour bond lengths, the result for the reported equilibrium configuration cannot be considered as reliable.

4.2. Pt_N, $N = 7$–10—octahedral motifs

For Pt clusters of this size, only a very few *ab initio* studies have been performed. Tian *et al* [109] reported a DFT calculation for a Pt heptamer. The equilibrium structure is a distorted square pyramid with two adatoms placed in front of one of the triangular facets (the structure may also be described as composed by two face-sharing distorted square prisms); a spin quintuplet ($S = 2$) is energetically slightly more favourable than an $S = 3$ state. The DFT studies of Lin *et al* [107] include the Pt_{10} cluster. A tetrahedral structure (with atoms at the vertices and in mid-edge positions) is reported to be locally stable (spin $S = 4$), but no extensive search for other possible structures has been performed. The equilibrium structures reported by Xiao and Wang [113] are a capped trigonal prism with $S = 1$ ($N = 7$), a cube with $S = 4$ ($N = 8$), a capped cube with $S = 3$ ($N = 9$), and a 10-atom tetrahedron with $S = 3$ ($N = 10$). Sebetci and Guvenc [119] have used classical MD and thermal quenching simulations, based on a semiempirical force field of the embedded-atom type, to search for global structural minima for Pt_N cluster with $N = 2$–21. The equilibrium structures are: a pentagonal bipyramid ($N = 7$); an octahedron with capping atoms on two triangular facets ($N = 8$); for $N = 9$–14 the minimum energy structures are based on the pentagonal bipyramid (including the icosahedron for Pt_{13}). However, the earlier work of Yang and DePristo [118] had shown that small changes in the force field can stabilize more open structures.

4.2.1. Pt_7. The locally stable structures of a Pt_7 cluster are a distorted centred hexagon (point group symmetry D_{2h}), a distorted pentagonal bipyramid (symmetry C_{2v}) and an octahedron with a capped triangular facet (symmetry C_{1h}) (see figure 20)—this structure in an $S = 4$ configuration represents the ground state. The structural energy differences relative to the two other configurations are relatively large.

While for the two metastable configurations all atoms are nonmagnetic in the $S = 0$ state and magnetically quite homogeneous in all $S \neq 0$ states, the capped octahedron is antiferromagnetic for $S = 0$ and shows a substantial spin-down component in the magnetization density for $S = 1$ and 2; see figure 21. The high-spin states are magnetically

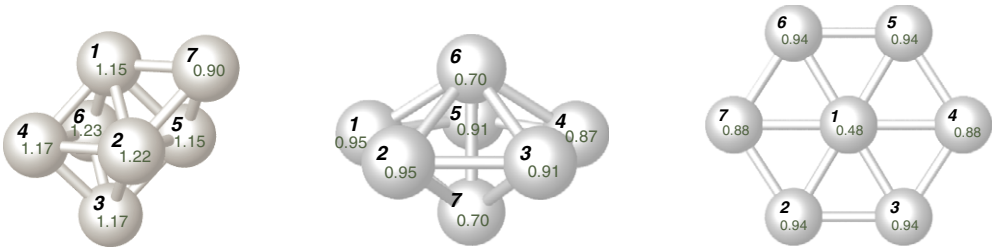

Figure 20. Structure and local magnetic moments of Pt_7 clusters in their three metastable configurations (from left to right): capped octahedron—point group symmetry C_{1h}, $S = 4$; pentagonal bipyramid—C_{2v}, $S = 3$; centred hexagon—D_{2h}, $S = 3$; cf text.

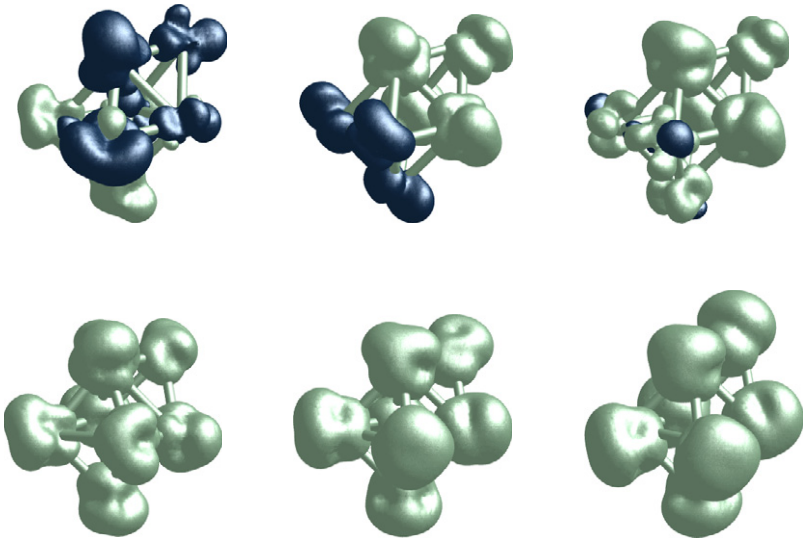

Figure 21. Isosurface plots of the magnetization densities for the six magnetic isomers of a Pt_7 cluster forming a capped octahedron with $S = 0$–5 (from top left to bottom right).

more homogeneous and for $S = 5$ the geometric structure also acquires a higher C_{3v} symmetry.

Previous studies of Pt clusters of this size may be found only in the work of Tian *et al* [109] and of Xiao and Wang [113]. The ground-state configuration proposed by Xiao and Wang is a trigonal prism with a capped triangular face (symmetry C_{3v}, $S = 1$), which is 10 meV/atom lower in energy than a strongly distorted capped octahedron (symmetry C_1, $S = 4$). Tian *et al* find a rather irregular structure consisting of two face-sharing square prisms with energetically nearly degenerate $S = 2$ and 3 states.

4.2.2. Pt_8. For the Pt_8 cluster two variants of an octahedron with two capped triangular faces represent the energetically most favourable structures; see figure 22. The two structures differ only by the choice of the triangular faces in front of which an adatom is placed—it turns out to be energetically more favourable to decorate two facets on opposite sides of the octahedron such that no bond between the adatoms is formed. This differs from the Ni_8 cluster where the other variant (which may be considered also as a bidisphenoid) is favoured. Both configurations are magnetically quite homogeneous in their ground state, but antiferromagnetic in their low-

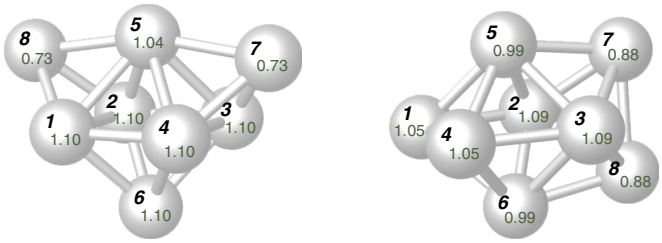

Figure 22. Structure and local magnetic moments of Pt_8 clusters forming an octahedron with two capped triangular faces, both with C_{2v} symmetry and $S = 4$. The structure shown at the left represents the ground state.

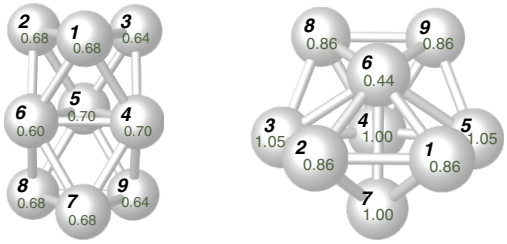

Figure 23. Structure and local magnetic moments of Pt_9 clusters (from left to right): double trigonal antiprism—C_{2v}, $S = 3$; capped pentagonal bipyramid—point group symmetry C_{1h}, $S = 4$; cf text.

spin isomers (for details see supporting material available at stacks.iop.org/JPhysCM/18/9703). A Pt_8 cube which forms the ground state according to previous studies [113] is found to be unstable.

4.2.3. Pt_9. For the Pt_9 cluster the two locally stable configurations. A pentagonal bipyramid with two capped triangular facets and a double trigonal antiprism (see figure 23) represent two competing principles of structure formation—polytetrahedral and polyoctahedral packing. The double trigonal antiprism (lower in energy by 52 meV/atom) may also be considered as composed by two distorted octahedra sharing a triangular face. It is quite remarkable that all magnetic isomers of this structure have a relatively high symmetry (D_{3h}), with the exception of the $S = 3$ ground state, where the symmetry is reduced to C_{2v} (for details see supporting material available at stacks.iop.org/JPhysCM/18/9703).

4.2.4. Pt_{10}. For the Pt_{10} cluster we have identified three locally stable structures: (a) a tetragonal antiprism with capped square faces, (b) a structure consisting of two distorted edge-sharing octahedra, and (c) a large tetrahedron with atoms occupying the vertices and mid-edge positions (see figure 24)—like for the Ni_{10} cluster, this last structure represents the ground state being favoured by at least 200 meV/atom. For the low-spin isomers ($S = 0, 1$) the symmetry is only C_{1h}, while for higher magnetic moments, the full tetrahedral symmetry (point group T) is recovered (for details, see supporting material available at stacks.iop.org/JPhysCM/18/9703). Xiao and Wang [113] have also found that the tetrahedron represents a stable structure for the Pt_{10} cluster, but report a $S = 3$ state. Lin *et al* have also examined the 10-atom tetrahedron and found the $S = 4$ state to be the ground state. The stabilizing principle of this structures is evidently the low surface energy of the close-packed facets.

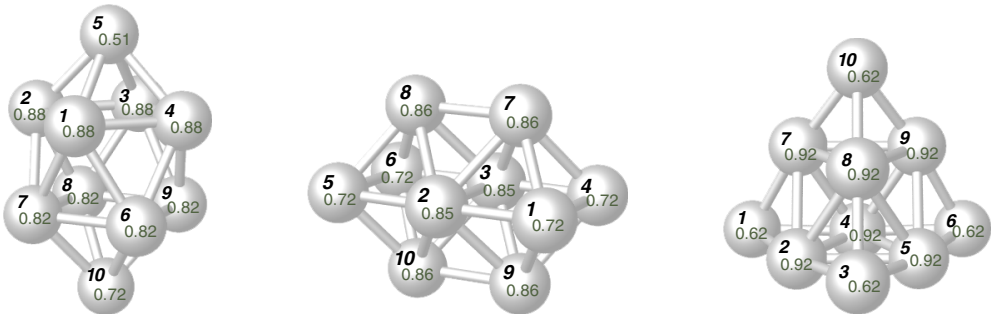

Figure 24. Structure and local magnetic moments of Pt_{10} clusters in their three metastable configurations (from left to right): capped tetragonal antiprism—point group symmetry C_{4v}, $S = 4$; edge-sharing octahedra—D_{2h}, $S = 4$; tetrahedron—T, $S = 4$; cf text.

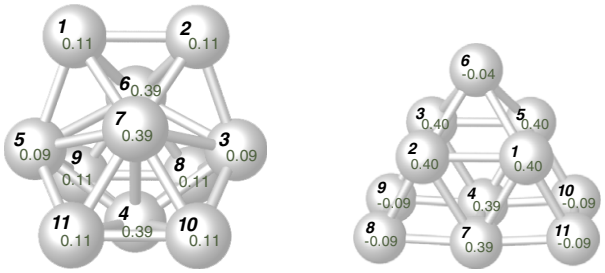

Figure 25. Structure and local magnetic moments of Pt_{11} clusters in two energetically degenerate configurations: polytetrahedral cluster (left)—point group symmetry C_{2v}, $S = 1$; pyramid (right)—C_{2v}, $S = 1$; cf text.

4.3. Pt_N, $N = 11$–13—polytetrahedral or polyoctahedral structures?

For cluster sizes approaching the magic number of $N = 13$, the question is whether the equilibrium structures are based on polytetrahedral motifs with pentagonal symmetry (culminating in the 13-atom icosahedron, as for Ni clusters) or whether other structures based on octahedral packing (as for Pd and Rh clusters) are stabilized. Previous DFT studies [104, 111–113] of Pt_{13} agree that the ground state is not an icosahedron but propose different more or less symmetric structures.

4.3.1. Pt_{11}. For the Pt_{11} cluster we have found two locally stable, energetically degenerate structural isomers (structural energy difference 1 meV/atom): (a) a polytetrahedral cluster (point group symmetry C_{2v}—essentially a pentagonal bipyramid with four adatoms capping symmetrically four triangular facets) and (b) an irregular pyramid (symmetry C_{2v}—describable as composed of three face-sharing trigonal prisms plus an adatom capping a rectangular facet); see figure 25. A polyoctahedral starting structure transforms into configuration (b) representing the ground state. The magnetic ground state is $S = 1$ in both cases; the magnetization density shows a strong ferrimagnetic component (for details, see supporting material available at stacks.iop.org/JPhysCM/18/9703). The transition from the high-spin state stable in the smaller clusters to a low-spin state is remarkable. In addition we note that the magnetic energy difference between the $S = 0$ and 1 states of configuration (b) is only 6 meV/atom.

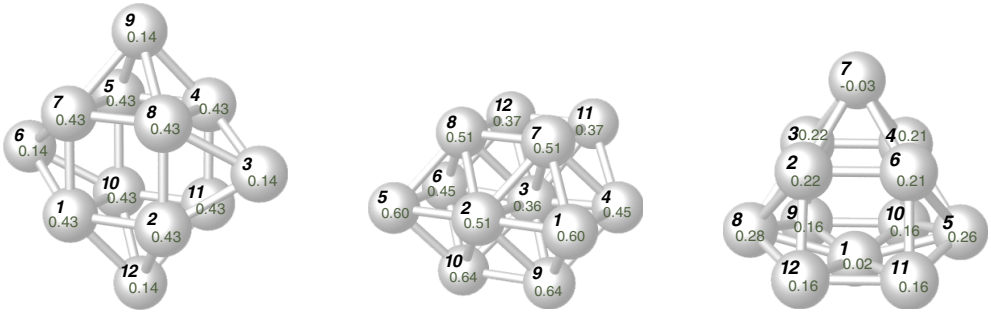

Figure 26. Structure and local magnetic moments of Pt_{12} clusters in their three metastable configurations (from left to right): capped cube—point group symmetry D_{4h}, $S = 2$; octahedral cluster—C_{1h}, $S = 3$; pyramid—C_{2v}, $S = 1$; cf text.

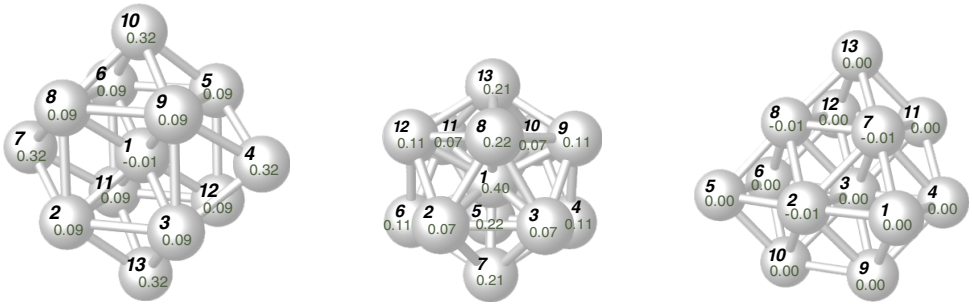

Figure 27. Structure and local magnetic moments of Pt_{13} clusters in their three metastable configurations (from left to right): capped cube—point group symmetry D_{4h}, $S = 1$; icosahedron—C_{2h}, $S = 1$; cluster of octahedra—C_{3v}, $S = 0$; cf text.

4.3.2. Pt_{12}. For the 12-atom Pt cluster we have found three locally stable structural isomers, see figure 26: (a) a distorted cube with four adatoms symmetrically arranged on rectangular facets (symmetry D_{4h}—$S = 2$), (b) a cluster of octahedra (C_{1h}—$S = 3$), and (c) a pyramid with seven atoms in a slightly buckled basis, four atoms in the next plane, and one on top (C_{2v}—$S = 1$)—this is the ground state. An incomplete icosahedron (with one vacant vertex) transforms into the equilibrium structure. The different spin states of the three structural isomers are not very relevant, since the magnetic energy differences are only a few meV.

4.3.3. Pt_{13}. For the Pt_{13} cluster we have found three locally stable configurations (see figure 27): (a) a centred cube with four symmetrically arranged capping atoms (point group symmetry D_{4h}—$S = 1$), (b) a distorted icosahedron (C_{2h}—$S = 1$), and (c) a cluster of three octahedra (C_{3v}—$S = 0$), also describable as a 'buckled biplanar' arrangement, i.e. as a stacking of two fragments of close-packed planes such as they exist in the fcc lattice of Pt metal. This last structure represents the ground state, the icosahedron being disfavoured by a large structural energy difference of 159 meV/atom. This result is remarkable for two respects. (a) The structure we find for the Pt_{13} is the same as the optimized structures for Pd_{13} and Rh_{13} reported in our previous work [60], and independently by Chang and Chou [65] for a series of 4d-metal clusters. (b) All structural isomers of Pt_{13} have a low-spin ground state, with only minimal magnetic energy differences relative to a nonmagnetic state. As the same result was

Table 4. Stable structure (point-group symmetry) for nickel, palladium and platinum clusters. If the lowest structural energy difference is less than 20 meV/atom, the structures of both isomers are listed.

N	Nickel	Palladium	Platinum
2	Dimer ($D_{\infty h}$)	Dimer ($D_{\infty h}$)	Dimer ($D_{\infty h}$)
3	Triangle (C_{2v})	Triangle (C_{2v})	Triangle (D_{3h})
4	Tetrahedron (S_4)	Tetrahedron (T_d)	Tetrahedron (C_{2v}) Rhombus (D_{2h})
5	Trig. bipyramid (D_{3h})	Trig. bipyramid (D_{3h}) Square pyramid (C_{4v})	Trig. bipyramid (D_{3h})
6	Octahedron (D_{4h})	Octahedron (O_h)	Square pyramid + adatom (C_{1h})
7	Octahedron + adatom (C_{3v})	Pentagonal bipyramid (C_{2v})	Octahedron + adatom (C_{1h})
8	Octahedron + 2 adatoms (C_{2v}) (Bidisphenoid) Octahedron + 2 adatoms (C_{2v})	Octahedron + 2 adatoms (C_{2v}) (Bidisphenoid)	Octahedron + 2 adatoms (C_{2v})
9	Capped pentag. bipyramid (C_{1h}) Double trig. antiprism (D_{3h})	Double trig. antiprism (C_{2v}) Capped pentag. bipyramid (C_{1h})	Double trig. antiprism (C_{2v})
10	Tetrahedron (T) (Trig. pyramid)	Edge-sharing octahedra (D_{2h})	Tetrahedron (T) (Trig. pyramid)
11	Polytetrah. cluster (C_{2v})	Edge-sharing octahedra (C_1) + adatom Polytetrah. cluster (C_{2v})	Pyramid (C_{2v}) Polytetrah. cluster (C_{2v})
12	Incompl. icosahedron (C_{5v}) Pyramid (C_{2v})	Edge-sharing octahedra (C_{1h}) + 2 adatoms Incomplete icosahedron (C_{5v})	Pyramid (C_{2v})
13	Icosahedron (C_{1h})	Cluster of octahedra (C_{1h}) Icosahedron (I_h)	Cluster of octahedra (C_{3v})

also found for the 11- and 12-atom Pt clusters, it is evident that magnetism begins to break down at this critical size.

5. Trends in the Ni–Pd–Pt group

5.1. Cluster geometry

We now turn to the discussion of trends in the Ni–Pd-series. We begin by comparing the cluster structures compiled in table 4. For the trimer, a small distortion of the equilateral triangle is noted for Ni and Pd, increasing with increasing moment. It is therefore not surprising that no distortion occurs for the low-spin Pt_3 cluster. For all three tetramers, the equilibrium structure is a tetrahedron—but perfect T_d symmetry is realized only for the Pd cluster, whereas the symmetry is broken for Ni and Pt. The symmetry lowering is more pronounced for the low-moment Pt_4 cluster, caused by the magnetic inequivalence of the Pt atoms (see figure 16). The $S = 1$ Pt tetrahedron is energetically almost degenerate with a planar geometry with $S = 2$. All pentamers form a trigonal bipyramid, but for Pd_5 a square pyramid is almost as low in energy. For the hexamer, Ni and Pd form an octahedron—perfect O_h symmetry is realized for the low-spin Pd_6 cluster; for the high-spin Ni_6 cluster the symmetry is reduced to tetragonal. For the heptamer both Ni and Pt form an octahedron with a capped triangular face, whereas this structure is unstable for Pd and transforms to a pentagonal bipyramid. For the octamer, slightly

different variants of a distorted octahedron with two capping atoms are stabilized, with only small structural energy differences.

For clusters with up to six atoms, our predictions agree with the Ni_N structures suggested on the basis of the chemical probe experiments, and for Ni as well as for Pd clusters, also with the results of earlier *ab initio* DFT calculations [79, 80, 83–85, 91] (for Pd clusters, see the detailed discussion in our previous publication). For Pt clusters our findings disagree with the planar geometries predicted by Yang *et al* [104] and Xiao and Wang [113]. It should be pointed out, however, that the near-degeneracy of tetrahedron and rhombus for Pt_4, and the higher stability of a square pyramid plus adatom for Pt_6, express a certain tendency towards less isotropic structures.

For the Ni heptamer our result agrees with Desmarais *et al* [81], but is in conflict with Nayak *et al* [86]; for the octamer we agree again with Desmarais *et al*. For both clusters, our results agree with the chemical probe experiments.

For Ni_9 and Pd_9, a capped pentagonal bipyramid and a double trigonal antiprism are energetically nearly degenerate, whereas the latter is favoured for Pt_9. As the former structure is a polytetrahedral cluster, whereas the latter may be considered as composed by two face-sharing octahedra, this near-degeneracy illustrates the competition between two building principles. Ni_{10} and Pt_{10} form a trigonal pyramid (or distorted tetrahedron) with atoms and the vertices and mid-edge positions—in this structure the cluster is bounded only by (111) facets and this may determine its stability. A bit surprisingly, Pd_{10} is an exception to the rule—the tetrahedron is metastable only in a strongly distorted form and higher in energy. For the 11-atom cluster, a polytetrahedral arrangement is energetically quite favourable for all three elements, with other structures being slightly lower in energy for Pd and Pt. The same competition between polytetrahedral (or icosahedral) and octahedral building principles is also evident for 12- and 13-atom clusters. Altogether we find a predominance of tetrahedral close-packing for the 3d-metal Ni and a tendency towards octahedral motifs closer to the fcc crystal structure for the heavier elements.

For clusters with 9 to 12 atoms, no previous structure optimizations based on *ab initio* calculations are available. For Ni_9 and Ni_{12} clusters, our predictions agree again with the interpretation of the molecular-uptake experiments, for 10- and 11-atom clusters no conclusive interpretation is available. The 13-atom cluster has been a much used testing-ground for theories of cluster structures. Our result of a Ni_{13} icosahedron agrees with earlier studies [79, 86–88], but the polyoctahedral (or 'buckled biplanar') structures for Pd_{13} and Pt_{13} clusters are a novel prediction. To a certain extent, this finding correlates with the predicted preference for planar arrangements on Au clusters of comparable size.

5.2. Binding energy and interatomic distances

The trends in binding energy, coordination number, interatomic distances, magnetic moment, and HOMO–LUMO gap are compiled in figure 28. For a given cluster size, binding is weakest for Pd, and stronger for Ni and Pt. For the dimer, this trend agrees with the experimental estimates derived by Lineberger *et al* [143, 145] from photoelectron spectroscopy. For Ni_2, Pd_2, and Pt_2 the calculated binding energies are 1.154, 0.646, and 1.492 eV/atom, to be compared with experimental estimates of 1.035, 0.515, and 1.57 eV/atom. Binding energies for larger Ni clusters in the range $N = 2$–18 have been derived by Lian *et al* [146] from results on the collision-induced dissociation (CID) of positively charged Ni_N^+ clusters and the known ionization energies of neutral Ni_N clusters, and assuming that the clusters dissociate via evaporation, i.e. sequential loss of Ni atoms. This analysis leads to an $N^{\frac{1}{3}}$-dependence of the binding energies (see also below), but the absolute values are hampered by an unrealistically

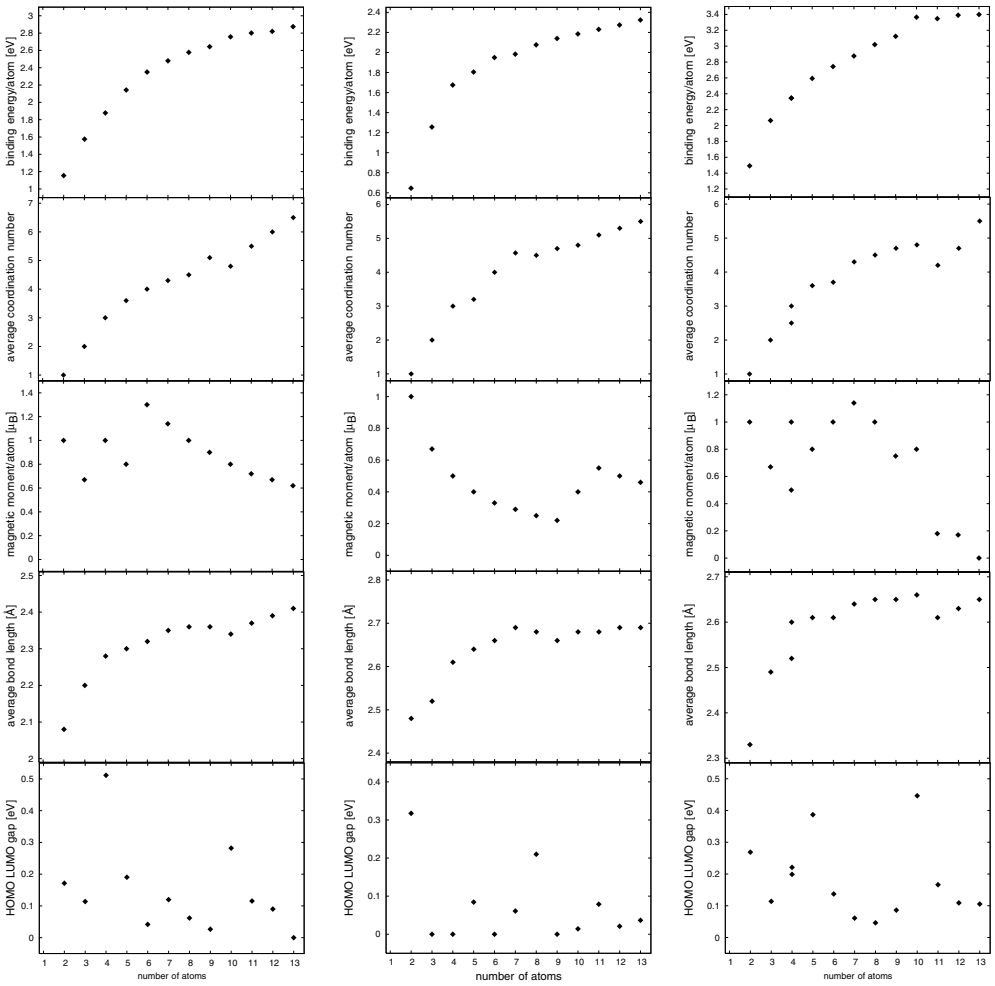

Figure 28. Binding energy, average coordination number, magnetic moment/atom, average bond length and HOMO–LUMO gap of energetically preferred Ni_N, Pd_N and Pt_N (from left to right) clusters with $N = 2 \rightarrow 13$.

large value assumed for the ionization energy of the dimer, leading to a anomalously low dissociation energy for the neutral trimer (0.82 eV, which is only about one third of that for the Ni_3^+ cluster-ion, while only minor differences are observed for all other cluster sizes). Using instead the value determined by Ervin *et al* [143, 145] for the $Ni_3 \rightarrow Ni_2 + Ni$ reaction (2.26 eV), we derive binding energies of 1.03/1.44/1.58/1.70/2.04 eV/atom for Ni_2 to Ni_6, to be compared with the theoretical values of 1.15/1.58/1.88/2.14/2.35 eV/atom for the same series. For larger clusters, the experimental binding energies increase continuously to 2.35 and 2.45 eV/atom for Ni_{12} and Ni_{13}, while theory yields 2.82 and 2.88 eV/atom, respectively. Hence the overbinding of the DFT becomes more pronounced for increasing cluster size.

Less information is available for large Pd and Pt clusters. For Pt_N clusters, Grushow and Ervin [147] derive binding energies of 1.57/2.51/3.16 eV/atom for $N = 2, 3, 4$, respectively, from CID experiments on negatively charged Pt clusters and estimates of the electron affinities,

but the results are affected by large uncertainties in the electron affinities of the trimer and tetramer. The corresponding theoretical results are 1.49/2.06/2.35 eV/atom—hence for the heavy Pt clusters, DFT produces a substantial underbinding. The trend in the binding energies of Ni, Pd, and Pt clusters agrees with the general observation on gradient-corrected DFT functionals: while for lighter elements such as Ni, the GGA does not completely cure the overbinding tendency of the LDA, the GGA corrections tend to overshoot for the heavy elements such as Pt.

The energy as a function of the cluster size increases almost monotonically towards the cohesive energy of the bulk material; unlike for simple-metal clusters there is no indication of an electronic shell structure (which would lead to a particular stability of an 8-atom cluster, due to a closed electron shell). For Ni, the binding energy is an entirely convex function of N and for Pt only the capped octahedral, antiprismatic and pyramidal structures for $N = 7, 9$ and $N = 11$ have a binding energy that is slightly lower than the average binding energy of clusters with $N \pm 1$. For the $N = 7$ and 9 structures a similar result had been found for Pd clusters; for Pt we note the outstanding binding energy of the large Pt_{10} tetrahedron. The variation of the binding energy with cluster size follows rather well two trends. (i) As a function of the cluster size, the binding energy varies (except for the dimer) as $E_{\mathrm{bind}} \propto N^{\frac{1}{3}}$—according to equation (1) this means that the major contribution to the binding energy comes from bonds along the edges of the cluster. The binding energies of the largest Pt clusters are slightly enhanced over this trend—this shows that the surface energies of the close-packed facets of these structures begin to play a role. (ii) The binding energy varies essentially as the square-root of the average coordination number, $E_{\mathrm{bind}} = \sqrt{N_{\mathrm{C}}}|h|$, where $|h|$ is an average hopping integral, as expected from the simplest tight-binding model. This reflects the important role of the formation of covalent bonds in determining binding energy and cluster structure.

The average interatomic distances are appreciably shorter than in the bulk metal. The interatomic distances increase at first rather rapidly with cluster size, and for Ni clusters this trend is continued up to $N = 13$, whereas for Pd and Pt, the increase is slowed down for $N \geqslant 7$. This is related to the fact that the interatomic distances in the equilibrium structures determined by dynamical simulated annealing are always considerably shorter that those in the highly symmetric cluster structures assumed in most earlier studies. For example, in a Pd_{13} cluster the average bond length in a distorted icosahedron is 2.65 Å, and only 2.59 Å in the stable buckled biplanar structure; in Pt_{13} the corresponding interatomic distances are 2.73 Å and 2.65 Å. In Ni_{13} where the stability is reversed, the difference in the interatomic distances is only 0.04 Å.

5.3. Magnetic moments

The evolution of the magnetic moment with cluster size shows some common trends, but also some characteristic differences. The magnetic ground state of all dimers and trimers is $S = 1$, but whereas for Pd the spin-triplet state is favoured up to Pd_9, for Ni and Pt high-spin isomers are favoured already for clusters of intermediate size. Ni_4 and Ni_5 clusters have a magnetic moment of $4\mu_{\mathrm{B}}$, Ni clusters with $N = 6$–13 have a constant moment of $8\mu_{\mathrm{B}}$. The comparison with the Stern–Gerlach experiments [51, 53] for $N \geqslant 5$ has already been discussed above. While a constant moment of $8\mu_{\mathrm{B}}$ reproduces the general trend quite well, the absolute values are too small by about 0.3–$0.4\mu_{\mathrm{B}}$/atom. A possible explanation for this deficit is a large contribution from the orbital moment—a theoretical verification will require fully relativistic calculations including spin–orbit coupling effects and noncollinear magnetic structures.

For Pt clusters, high-spin states with $S = 2$–8 represent the stable magnetic isomers for clusters with $N = 4$–10 where octahedral motifs determine the cluster structure, i.e. in this

range Pt clusters tend to be more magnetic than Pd clusters. For larger Pt clusters, the magnetic moment effectively breaks down—if the ground state remains magnetic, the energy difference relative to the nonmagnetic state is only minimal.

6. Conclusions

This paper completes an extensive investigation of the formation of structural and magnetic isomers of small clusters of the metals of the Ni group. Our results emphasize the importance of directional covalent bonds in determining the trends in the binding energy and in the geometric structure of the clusters. For the binding energy we predict a smooth increase as a function of cluster size, in contrast to the discontinuous variation characteristic for simple-metal clusters arising from particular stability of clusters with filled electronic shells. We find that the binding energy follows a square-root dependence on the average coordination number (as expected on the basis of simple tight-binding arguments) and a cube-root dependence on the number of atoms in the cluster (reflecting the fact that for these small cluster sizes almost all interatomic bonds are along edges of the cluster). The $N^{\frac{1}{3}}$-dependence of the binding energy is in good agreement with the experimental estimates of Lian *et al* [146] for Ni clusters.

For the cluster structure, our present results for Pt clusters confirm and extend the surprising result of our studies of Pd clusters and Rh clusters [60] that the ground-state configuration of 13-atom clusters is not an icosahedron, but rather a polyoctahedral configuration describable also as a 'buckled biplanar' arrangement [65] consisting of two fragments of close-packed lattice planes. In contrast, the ground-state configuration of a Ni_{13} cluster is an icosahedron, and polytetrahedral packing is also the dominant principle determining the structure of Ni clusters with 12 and 11 atoms. For the smallest clusters of 5d metals, a tendency to adopt planar structures has been postulated. This is not confirmed by our calculations for Pt clusters—except for a very small energy difference between a tetrahedral and a flat structure for Pt_4. It is also necessary to emphasize that except for the smallest clusters, static energy-minimization methods are insufficient for the exploration of configuration space—many of our ground-state configurations could only be identified by the combination of *ab initio* molecular dynamics and dynamical simulated annealing methods.

Our fixed-moment calculations demonstrate that geometric and magnetic structures are strongly coupled. Increasing magnetic moment and increasing exchange splitting and hence to a change of population of the spin-polarized cluster orbitals—our results offer several striking examples of the variation of point-group symmetry with magnetic moment. For Ni clusters we find a strong tendency towards the formation of ferrimagnetic ordering in many low-spin isomers. The smallest Pt clusters are also magnetic, but we found that magnetism begins to break down already for clusters with nine or more atoms—the Pt_{13} cluster is already nonmagnetic.

The determination of the size of the cluster moment remains a challenge for density-functional calculations. For Ni_N clusters, where precise determinations of the cluster moments for $N \geqslant 6$ are available from Stern–Gerlach experiments [51, 53] our results reproduce the correct trend, but the absolute values of the magnetic moments are too small by about $0.4\mu_B$. Two mechanisms have been invoked to explain the discrepancy: (i) strong electronic correlation effects, and (ii) a large orbital contribution arising from spin–orbit coupling. To examine (i), we have confronted our density-functional results with those of quantum-chemical studies treating electronic correlation at a higher level of theory. However, most calculations at the HF-CI or MRCI levels are hampered by the fact that structural optimization of the cluster is beyond what is computationally feasible and that except for the very smallest clusters, basis-set convergence is very difficult to achieve. At the moment there is no firm indication that quantum-chemical

approaches produce higher moments than DFT calculations. Guirado *et al* [139] and Wan *et al* [140] have claimed that spin–orbit coupling can lead to the formation of a large orbital moment and that the orbital contribution closes the gap between theory and experiment. However, both calculations are based on empirical tight-binding Hamiltonians, and use very different values of the on-site Coulomb repulsion U to achieve a moment in agreement with experiment. We have completed a few preliminary fully relativistic DFT calculations for the smallest Ni and Pt clusters. The results show that spin–orbit coupling leads in many cases to a noncollinear magnetic structure, and that a simultaneous optimization of the structural and magnetic degrees of freedom is mandatory. This leads to an extreme computational effort. We have evidence for a substantial orbital moment, but at the moment the results have not yet extended to cluster sizes where experimental results are available.

Acknowledgments

This work has been supported by the Austrian Science Funds (Fond zur Förderung der wissenschaftlichen Forschung in Österreich—FWF) through the Science College 'Computational Materials Science'.

References

[1] Nalwa H S (ed) 2004 *Encyclopedia of Nanoscience and Nanotechnology* (New York: American Scientific)
[2] Khanna S N and Castleman A W (ed) 2003 *Quantum Phenomena in Clusters and Nanostructures* (Heidelberg: Springer)
[3] Henry C R 1998 *Surf. Sci. Rep.* **31** 235
[4] Knickelbein M B 1999 *Annu. Rev. Phys. Chem.* **50** 79
[5] Sun S, Murray C B, Weller D, Folks L and Moser A 2000 *Science* **287** 1989
[6] Cleveland C L and Landman U 1991 *J. Chem. Phys.* **94** 7376
[7] Baletto F and Ferrando R 2005 *Rev. Mod. Phys.* **77** 371
[8] Baletto F, Mottet C and Ferrando R 2002 *Chem. Phys. Lett.* **354** 82
[9] Mackay A L 1962 *Acta Crystallogr.* **15** 916
[10] Martin T P 1996 *Phys. Rep.* **273** 199
[11] Marks L D 1994 *Rep. Prog. Phys.* **57** 603
[12] Farges J, de Feraudy M F, Raoult B and Torchet G 1986 *J. Chem. Phys.* **84** 3491
[13] Reinhard D, Hall B D, Berthoud P, Valkealahti S and Monot R 1998 *Phys. Rev.* B **58** 4917
[14] Doye J P K and Wales D J 1995 *J. Chem. Phys.* **112** 9659
[15] Knight W D, Clemenger K, de Heer W A, Saunders W A, Chou M Y and Cohen M L 1984 *Phys. Rev. Lett.* **52** 2141
[16] Roethlisberger U and Andreoni W 1991 *J. Chem. Phys.* **94** 8129
[17] Spiegelman F, Poteau R, Montag B and Reinhard P G 1998 *Phys. Lett.* A **242** 163
[18] Zhao J, Luo Y and Wang G 2001 *Eur. Phys. J.* D **14** 309
[19] Mottet C, Goniakowski J, Baletto F, Ferrando R and Tréglia G 2004 *Phase Transit.* **77** 101
[20] Rosato M G V and Legrand B 1989 *Phil. Mag.* A **59** 321
[21] Doyle J P K and Wales D J 1998 *New J. Chem.* **22** 733
[22] Sutton A P and Chen J 1990 *Phil. Mag. Lett.* **61** 139
[23] Alonso J A 2000 *Chem. Rev.* **100** 637
[24] Bauschlicher C W, Langhoff S R and Partridge H 1990 *J. Chem. Phys.* **93** 8133
[25] Bonacic-Koutecky V, Cespiva L, Fantucci P and Koutecky J 1993 *J. Chem. Phys.* **98** 7981
[26] Bonacic-Koutecky V, Cespiva L, Fantucci P, Pittner J and Koutecky J 1994 *J. Chem. Phys.* **100** 490
[27] Jug K, Zimmermann B, Calaminici P and Koester A M 2002 *J. Chem. Phys.* **116** 4497
[28] Jug K, Zimmermann B and Koester A M 2002 *Int. J. Quantum Chem.* **90** 594
[29] Fujima N and Yamaguchi T 1989 *J. Phys. Soc. Japan* **58** 1334
[30] Massobrio C, Pasquarello A and Car R 1995 *Chem. Phys. Lett.* **238** 215
[31] Fournier R 2001 *J. Chem. Phys.* **115** 2165
[32] Oviedo J and Palmer R E 2002 *J. Chem. Phys.* **117** 9548
[33] Matulis V E, Ivashkevich O A and Gurin V S 2003 *J. Mol. Struct.: THEOCHEM* **664** 291

[34] Jennison D R, Schultz P A and Sears M P 1997 *J. Chem. Phys.* **106** 1856
[35] Liu Z F, Yim W L, Tse J S and Hafner J 2000 *Eur. Phys. J.* D **10** 105
[36] Gilb S, Weis P, Furche F, Ahlrichs R and Kappes M M 2002 *J. Chem. Phys.* **116** 4094
[37] Furche F, Ahlrichs R, Weis P, Jacob C, Gilb S, Bierweiler T and Kappes M M 2002 *J. Chem. Phys.* **117** 6982
[38] Hakkinen H, Moseler M and Landman U 2002 *Phys. Rev. Lett.* **89** 033401
[39] Hakkinen H, Yoon B, Landman U, Li X, Zhai H-J and Wang L-S 2003 *J. Phys. Chem.* A **107** 6168
[40] Bulusu S, Li X, Wang L-S and Zeng X-C 2006 *Proc. Natl Acad. Sci.* **103** 8326
[41] Car R and Parinello M 1985 *Phys. Rev. Lett.* **55** 2471
[42] Kresse G and Hafner J 1993 *Phys. Rev.* B **47** 558
[43] Kresse G and Hafner J 1994 *Phys. Rev.* B **49** 14251
[44] Bravo-Perez G, Garzon I L and Novaro O 1999 *J. Mol. Struct.: THEOCHEM* **493** 225
[45] Bravo-Perez G, Garzon I L and Novaro O 1999 *Chem. Phys. Lett.* **313** 655
[46] Wang J L, Wang G H and Zhao J J 2002 *Phys. Rev.* B **66** 035418
[47] Bonacic-Koutecky V, Burda J, Mitric R, Ge M, Zampella G and Fantucci P 2002 *J. Chem. Phys.* **117** 3120
[48] Li J, Li X, Zhai H J and Wang L S 2003 *Science* **299** 864
[49] Wang J L, Wang G H and Zhao J J 2003 *Chem. Phys. Lett.* **380** 716
[50] Billas I, Becker J, Chatelain A and de Heer W 1993 *Phys. Rev. Lett.* **71** 4067
[51] Apsel S E, Emmert J W, Deng J and Bloomefield L A 1996 *Phys. Rev. Lett.* **76** 1441
[52] Billas I, Chatelain A and de Heer W A 1997 *J. Magn. Magn. Mater.* **168** 64
[53] Knickelbein M B 2002 *J. Chem. Phys.* **116** 9703
[54] Xie Y and Blackman J A 2003 *J. Phys.: Condens. Matter* **15** L615
[55] Douglass D C, Bucher J P and Bloomfield L A 1992 *Phys. Rev.* B **45** 6341
[56] Cox A J, Louderback J G and Bloomfield L A 1993 *Phys. Rev. Lett.* **71** 923
[57] Cox A J, Louderback J G, Apsel S E and Bloomfield L A 1994 *Phys. Rev.* B **49** 12295
[58] Ganteför G and Eberhardt W 1996 *Phys. Rev. Lett.* **76** 4975
[59] Taniyama T, Ohta E and Sato T 1997 *Europhys. Lett.* **38** 195
[60] Futschek T, Marsman M and Hafner J 2005 *J. Phys.: Condens. Matter* **17** 5927
[61] Kumar V and Kawazoe Y 2002 *Phys. Rev.* B **66** 144413
[62] Moseler M, Häkkinen H, Barnett R N and Landman U 2001 *Phys. Rev. Lett.* **86** 2545
[63] Jinlong Y, Toigo F and Kelin W 1994 *Phys. Rev.* B **50** 7915
[64] Wang L and Ge Q 2002 *Chem. Phys. Lett.* **366** 368
[65] Chang C M and Chou M Y 2004 *Phys. Rev. Lett.* **93** 133401
[66] Khanna S N, Beltran M and Jena P 2001 *Phys. Rev.* B **64** 235419
[67] Liu S R, Zhai H J and Wang L S 2002 *Phys. Rev.* B **65** 113401
[68] Liu S R, Zhai H J and Wang L S 2002 *J. Phys. Chem.* **117** 9758
[69] Gerion D, Hirt A, Billas I, Chatelain A and de Heer W A 2000 *Phys. Rev.* B **62** 7491
[70] Morenzin J, Kietzmann H, Bechthold P S, Gantefor G and Eberhardt W 2000 *Pure Appl. Chem.* **72** 2149
[71] Parks E K, Zhu L, Ho J and Riley S J 1994 *J. Phys. Chem.* **100** 7206
[72] Parks E K, Kerns K P and Riley S J 2000 *J. Chem. Phys.* **112** 3384
[73] Kerns K P, Parks E K and Riley S J 2000 *J. Chem. Phys.* **112** 3394
[74] Scheer M, Brodie C A, Bilodeau R C and Haugen H K 1998 *Phys. Rev.* A **58** 2051
[75] Parks E K, Zhu L, Ho J and Riley S J 1993 *Z. Physik* D **26** 41
[76] Basch H, Newton M D and Moskovitz J W 1980 *J. Chem. Phys.* **73** 4492
[77] Estiu G L and Zerner M C 1996 *J. Phys. Chem.* **100** 16874
[78] Estiu G L 2000 *J. Phys. Chem.* A **104** 233
[79] Reuse F A and Khanna S N 1995 *Chem. Phys. Lett.* **234** 77
[80] Reuse F A and Khanna S N 1995 *Phys. Rev.* B **52** 11650
[81] Desmarais N, Jamorski C, Reuse F A and Khanna S N 1998 *Chem. Phys. Lett.* **294** 480
[82] Reuse F A and Khanna S N 1999 *Eur. Phys. J.* D **6** 77
[83] Castro M, Jamorski C and Salahub D R 1997 *Chem. Phys. Lett.* **271** 133
[84] Michelini M C, Diez R P and Jubert A H 1999 *J. Mol. Struct.: THEOCHEM* **490** 181
[85] Michelini M C, Diez R P and Jubert A H 2001 *Int. J. Quantum Chem.* **85** 22
[86] Nayak S K, Khanna S N, Rao B K and Jena P 1997 *J. Phys. Chem.* A **101** 1072
[87] Reddy B V, Nayak S K, Khanna S N, Rao B K and Jena P 1998 *J. Phys. Chem.* A **102** 1748
[88] Calleja M, Rey C, Alemany M M, Gallego L J, Ordejon P, Sanchez-Portal D, Artacho E and Soler J M 1999 *Phys. Rev.* B **60** 2020
[89] Barden C J, Rienstra-Kiracofe J C and Schaefer H F 2000 *J. Chem. Phys.* **113** 690
[90] Kruger S, Seemuller T J, Worndle A and Rosch N 2000 *Int. J. Quantum Chem.* **80** 567

[91] Duan H M, Gong X G, Zheng Q Q and Lin H Q 2001 *J. Appl. Phys.* **89** 7308
[92] Ruette F and Gonzalez G 2002 *Chem. Phys. Lett.* **359** 428
[93] Andriotis A N and Menon M 1998 *Phys. Rev.* B **57** 10069
[94] Fthenakis Z, Andriotis A N and Menon M 2003 *J. Chem. Phys.* **119** 10911
[95] Aguilera-Granja F, Bouarab S, Lopez M J, Iniguez M P and Alonso J A 1998 *Phys. Rev.* B **57** 12469
[96] Hernandez-Torres F A-G J and Vega A 2001 *Solid State Commun.* **117** 477
[97] Luo C 2000 *Modelling Simul. Mater. Sci. Eng.* **8** 95
[98] Luo C 2002 *Modelling Simul. Mater. Sci. Eng.* **10** 13
[99] Grigoryan V G and Springborg M 2004 *Phys. Rev.* B **70** 205415
[100] Xiang Y, Sun D Y and Gong X G 2000 *J. Phys. Chem.* A **104** 2746
[101] Ramaker D E, Oudenhuijzen M K and Koningsberger D C 2005 *J. Phys. Chem.* B **109** 5608
[102] Yeon-Wook K, Hong-Min L and Kelly T F 1989 *Acta Metall.* **37** 247
[103] Contrata W, Mitchell M J and Mochel J M 1993 *Ultramicroscopy* **48** 297
[104] Yang S H, Drabold D A, Adams J B, Ordejon P and Glassford K 1997 *J. Phys.: Condens. Matter* **9** L39
[105] Fortunelli A 1999 *J. Mol. Struct.: THEOCHEM* **493** 233
[106] Gronbeck H and Andreoni W 2000 *Chem. Phys.* **262** 1
[107] Lin X, Ramer N J, Rappe A M, Hass K C, Schneider W F and Trout B L 2001 *J. Phys. Chem.* **105** 7739
[108] Li T and Balbuena P B 2001 *J. Phys. Chem.* B **105** 9943
[109] Tian W Q, Ge M, Sahu B R, Wang D, Yamada T and Mashiko S 2004 *J. Phys. Chem.* A **108** 3806
[110] Cui Q, Musaev D G and Morokuma K 1998 *J. Phys. Chem.* A **102** 6373
[111] Watari N and Onishi S 1998 *Phys. Rev.* B **58** 1665
[112] Fortunelli A and Apra E 2003 *J. Phys. Chem.* A **107** 2934
[113] Xiao L and Wang L 2004 *J. Phys. Chem.* A **108** 8605
[114] Dai D and Balasubramanian K 1995 *J. Chem. Phys.* **103** 648
[115] Majumdar D, Dai D and Balasubramanian K 2000 *J. Chem. Phys.* **113** 7919
[116] Majumdar D, Dai D and Balasubramanian K 2000 *J. Chem. Phys.* **113** 7928
[117] Garcia-Rodeja J, Rey C, Gallego L J and Alonso J A 1994 *Phys. Rev.* B **49** 8495
[118] Yang L and DePristo A E 1994 *J. Chem. Phys.* **100** 725
[119] Sebetci A and Guvenc Z B 2003 *Surf. Sci.* **525** 66
[120] Kresse G and Furthmüller J 1996 *Phys. Rev.* B **54** 11169
[121] Kresse G and Furthmüller J 1996 *Comput. Mater. Sci.* **6** 15
[122] Wood D M and Zunger A 1985 *J. Phys. A: Math. Gen.* **18** 1343
[123] Perdew J P and Zunger A 1981 *Phys. Rev.* B **23** 5048
[124] Ceperley D M and Alder B J 1980 *Phys. Rev. Lett.* **45** 566
[125] Perdew J P and Wang Y 1992 *Phys. Rev.* B **45** 13244
[126] van Barth U and Hedin L 1972 *J. Phys. C: Solid State Phys.* **5** 1629
[127] Vosko S H, Wilk L and Nusair M 1980 *Can. J. Phys.* **58** 1200
[128] Blöchl P E 1994 *Phys. Rev.* B **50** 17953
[129] Kresse G and Joubert D 1999 *Phys. Rev.* B **59** 1758
[130] Dederichs P H, Blugel S, Zeller R and Akai H 1984 *Phys. Rev. Lett.* **53** 2512
[131] Mohn P and Schwarz K 1984 *J. Phys. F: Met. Phys.* **14** L129
[132] Stillinger F H and Weber T A 1984 *J. Chem. Phys.* **80** 4434
[133] Jaswal S S and Hafner J 1988 *Phys. Rev.* B **38** 7311
[134] Pinegar J C, Langenberg J D, Arrington C A, Spain E M and Morse M D 1995 *J. Chem. Phys.* **102** 666
[135] Ho J, Polak M L, Erwin K M and Lineberger W C 1986 *J. Chem. Phys.* **99** 8542
[136] Morse M D, Hansen G P, Landridge-Smith P R, Zeng L S, Gensic M E, Michalopoulos D L and Smalley R E 1984 *J. Chem. Phys.* **80** 5400
[137] Moskovitz M and Hulse J E 1977 *J. Chem. Phys.* **66** 3988
[138] Gajdos M, Eichler A and Hafner J 2004 *J. Phys.: Condens. Matter* **16** 1141
[139] Guirado-Lopez R A, Dorantes-Davila J and Pastor G M 2003 *Phys. Rev. Lett.* **90** 226402
[140] Wan X, Zhou L, Dong J, Lee T L and Wang D 2004 *Phys. Rev.* B **69** 174414
[141] Balasubramanian K 1987 *J. Chem. Phys.* **87** 6573
[142] Gupta S K, Nappi B M and Gingerich K A 1981 *Inorg. Chem.* **20** 966
[143] Ervin K M, Ho J and Lineberger W C 1988 *J. Chem. Phys.* **89** 4514
[144] Wang H and Carter E A 1992 *J. Phys. Chem.* **96** 1197
[145] Ho J, Polak M L, Ervin K M and Lineberger W C 1993 *J. Chem. Phys.* **99** 8542
[146] Lian L, Su C X and Armentrout P B 1992 *J. Chem. Phys.* **96** 7542
[147] Grushow A and Ervin K M 1997 *J. Chem. Phys.* **106** 9580